EUROPEAN COMMISSION

Community Research

SEVENTH FRAMEWORK PROGRAMME

CARBOWASTE

Treatment and Disposal of Irradiated Graphite and Other Carbonaceous Waste

Grant Agreement Number:

Technical Report T-3.2.1-b

Multiscale Structural Characterisation of Nuclear Graphite

Author(s): **Mohamed Ramzi Ammar and Jean-Noël Rouzaud (ENS)**

Reporting period: e.g. 01/04/2008– 23/11/2011

Date of issue of this report: 31/03/2013

Project co-funded by the European Commission under the Seventh Framework Programme (2007 to 2011) of the European Atomic Energy Community (EURATOM) for nuclear research and training activities

Dissemination Level

Start date of project: **01/04/2008** Duration: 48 **Months**

PU	Public	
RE	Restricted to the partners of the CARBOWASTE project	
CO	Confidential, only for specific distribution list defined on this document	**X**

Distribution list

Person and organisation name and/or group	Comments
All Carbowaste Partners	

CARBOWASTE		
Work package: 3 **Task: :** 3.2	**CARBOWASTE document no:** CARBOWASTE-1303-D-3.2.1-a (e.g. May 2008 as date of issue: 0805)	**Document type:** Deliverable
Issued by: ENS (UK) **Internal no.:** CW-3-2-1-b-T-c-F.pdf		**Document status:** Final

Document title

Multiscale Structural Characterisation of Nuclear Graphite

Executive summary

Revisions

Rev.	Date	Short description	Author	Internal Review	Task Leader	WP Leader
01	23/11/2011	1st Issue	*Mohamed Ramzi Ammar and Jean-Noël Rouzaud (ENS)*			

Contents

Figures

Tables

1 Introduction - background to the problem

The first generation of nuclear reactors in France was developed in the 1950s-1960s and consisted of graphite-moderated, gas-cooled reactors (GCR) using natural uranium. This technology seemed to be the right choice for a country like France with its natural (non-enriched) uranium reserves, allowing the use of moderators, such as graphite or heavy water, with only a slight neutron-absorbing effect. This technology, however, proved to have drawbacks as well as advantages. GCR reactors require high-purity graphite and refuelling is a complex operation. They are also larger and more expensive than water-cooled reactors, which use enriched uranium. For these reasons, France abandoned GCR technology as of 1969 in favour of the pressurised water reactor (PWR) system, under American licence. Dismantling these reactors, however, generates significant amounts (around 23,000 tonnes) of radioactive carbonaceous waste in France (see Figure 1 for the location of storage sites). This waste is known as low-level long-lived waste or LLW-LL, because it contains long-lived radioisotopes, such as ^{36}Cl (half-life = 300,000 years), which is produced by neutron activation of ^{35}Cl when the graphite is loaded in the reactor. If suitable procedures and treatment methods are to be found for decontaminating and/or disposing of nuclear graphite, the acquisition of structural data on graphite before and after irradiation is both fundamental and crucial.

Figure 1 –Radioactive graphite waste storage sites in France

In 1997, Andra began to collaborate with several French organisations, including the CEA, EDF and CNRS, to carry out research into 'graphite' waste treatment. 'Carbowaste', a European project involving 28 organisations and laboratories, was kicked off in May 2008. Within the context of this project, Andra signed a contract in autumn 2008 with LG-ENS, the Geology Laboratory of *Ecole Normale Supérieure* in Paris, UMR CNRS-ENS No. 8538.
Our research concerns the multiscale characterisation of nuclear graphite, before and after neutron irradiation, using the principal investigatory techniques available, including X-ray diffraction (XRD), Raman microspectrometry and transmission electron microscopy (TEM), especially HRTEM, its high-resolution mode. HRTEM is used for direct observation of how these carbons are organised, to try to image and quantify, on a nanometric scale, radiation-induced damage to their crystalline structure.

Pending the acquisition of irradiated samples, then while the samples were being studied, LG-ENS set up a collaborative initiative with INPL, the Institute of Nuclear Physics of Lyon (with Claire-Emilie Vaudey, Nelly Toulhoat, Nathalie Montcoffre) to study graphite samples implanted with ^{37}Cl, a non-radioactive element, as a means of studying graphite behaviour and structural changes induced by ion irradiation.

This final report brings together all the results obtained over the past two years concerning two types of nuclear graphite - Marcoule (G2) and Saint Laurent A2 (SLA2) under the following conditions: virgin, implanted (SLA2) and irradiated with neutrons during reactor operation (G2 and SLA2).

2 Brief bibliographical overview of graphite and carbon structure

Graphite is a crystalline allotrope of carbon, made up exclusively of sp^2 hybridised carbons. As shown in Figure 2, the graphite crystal belongs to the hexagonal system and consists of a compact stacking (AB stacks) of polycyclic aromatic layers (graphene layers). Natural graphite is generally found in metamorphic rock in the form of crystals, less than one micron in size, inside millimetric flakes. In addition, synthetic graphite has been produced on an industrial scale for more than a century, using heat treatment – at temperatures up to 2800-3000°C - to transform graphitisable carbon, such as petroleum coke and coal tar pitch into graphitic carbon. These graphite blocks display good mechanical properties and chemical inertness.

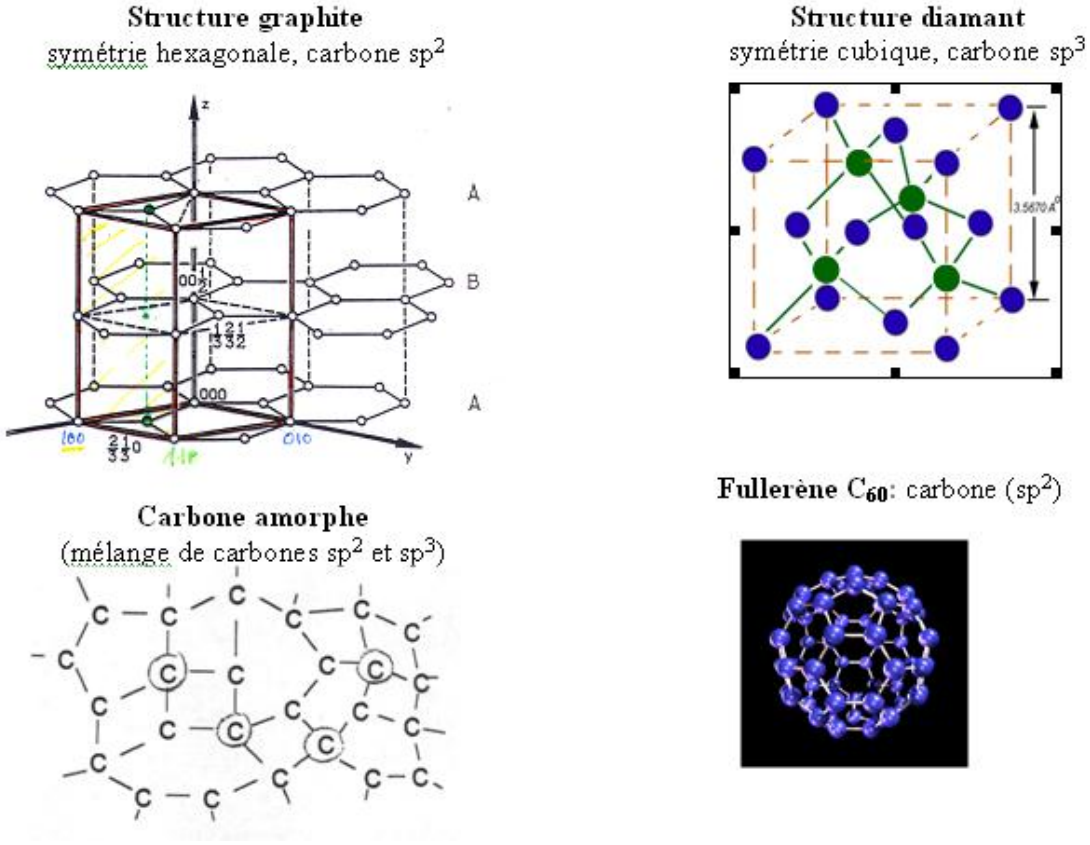

Figure 2 – Different carbon structures

Other allotropes of carbon (Figure 2) are: diamond (with a crystalline structure composed solely of sp^3 carbons); amorphous carbon (consisting of carbon atoms randomly distributed i.e.

without no crystalline order, not even local order, usually due to a random mixture of sp^2 and sp^3 hybridised carbons); and various forms of 'exotic' carbons, such as fullerenes and nanotubes, which were discovered in the 1980s, and composed for the most part of sp^2 carbons.

In addition, there is a vast family of nanostructured carbons, characterised by the existence of an order on a nanometric scale (with the presence of nanometric polyaromatic structural units, some of which are encircled in red in Figure 3). The carbon nanostructure (formerly known as microtexture) is determined by the spatial arrangement of these units. It depends on the chemical characteristics of the precursor (especially the oxygen-to-carbon ratio) and the formation conditions (pyrolysis temperature, possible mechanical stress, etc.). The nanostructure governs the mechanical properties of these carbons, as well as their graphitisability and reactivity. The examples below show two very different nanostructures - one porous, the other concentric – resulting from different precursors (wood, gaseous hydrocarbons) with an equivalent formation temperature (1000°C).

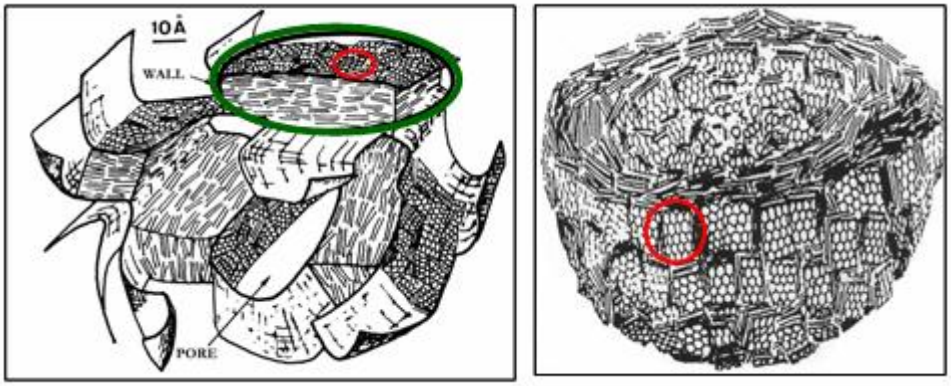

Figure 3 – Examples of nanostructured carbons: (porous on the left, example of an adsorbent carbon; concentric on the right, example of a soot)

For graphitisable carbons, the cokes obtained from oxygen-free precursors, such as anthracene, petroleum and coal-tar pitch, are formed from domains in which the structural units are oriented within volumes measuring several cubic micrometers (μm^3).

Figure 4 illustrates how graphitisation is induced solely by temperature, during a heat treatment process at 3000°C. As the temperature rises, the orientation of the structural units gradually improves and various types of structural defect are eliminated, leading to larger and

better stacked layers. The AB (tri-periodic) stacking order, which is characteristic of graphite, develops within these stacks when the temperature rises above 2000°C.

This diagram is based on TEM images allowing direct observation of the graphene layers in profile (left: high-resolution image) and graphite crystallite growth (bottom right: 110 dark field mode) **[1]**.

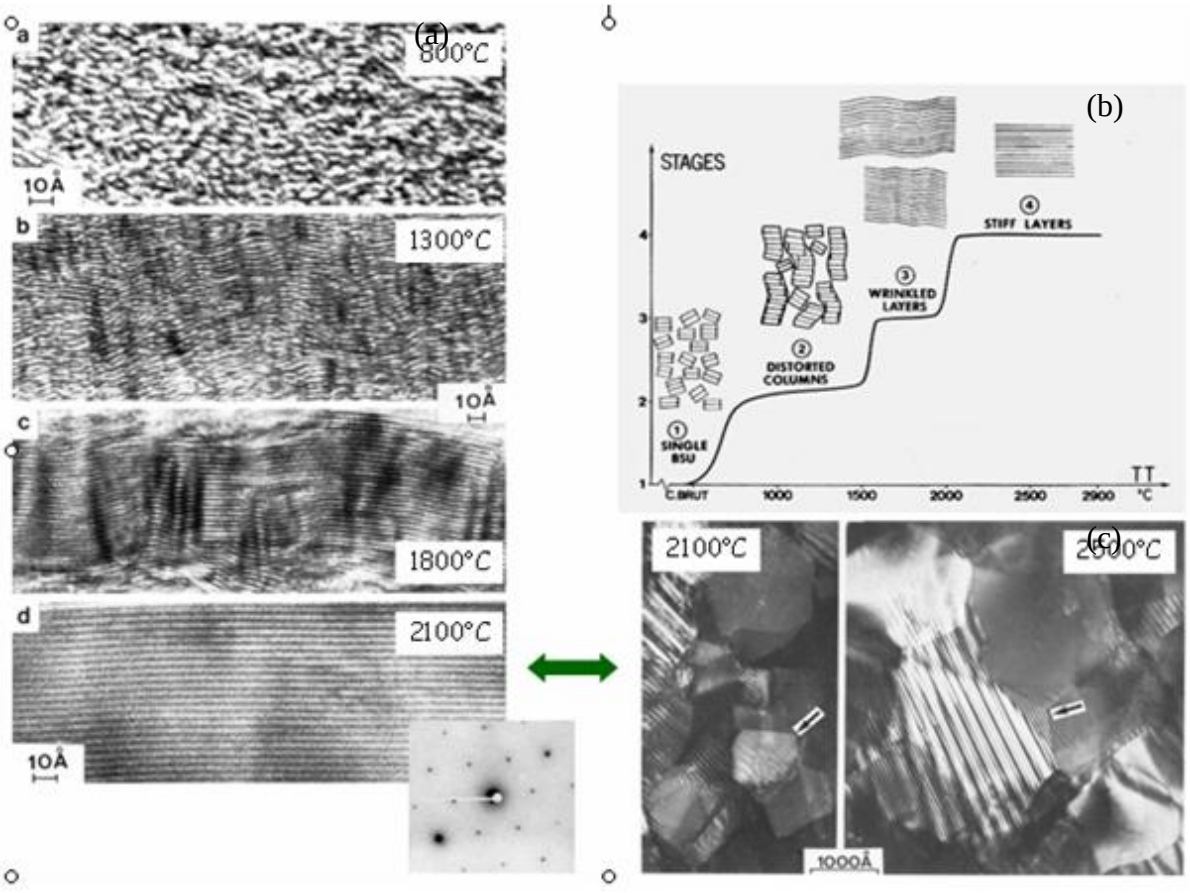

Figure 4 – Graphitisation of graphitisable carbons: (a) HRTEM images, (b) graphitisation diagram, (c) TEM images in 110 dark field mode showing how graphite crystallites grow as the temperature increases; from Rouzaud et al, 1983, 1989.

Nuclear reactors use a synthetic polycrystalline graphite. This is a carbon-carbon composite made up of a filler (generally calcined petroleum coke) and a binder (generally coal-tar pitch). It is made using the process shown in the diagram (Figure 5, reproduced by kind permission of Jean-Pierre Bonal, CEA, Saclay). First, the calcined coke is ground and

screened. The grains obtained are then mixed in suitable proportions to obtain the required density and to help expel the volatile matter from the binder. The coke is then mixed with coal-tar pitch at a temperature of 165°C, before being shaped by extrusion or unidirectional or isostatic compression. It is then baked at 800°C to 1200°C to coke the binder. The density and mechanical properties of the resulting product can then be enhanced through one or more impregnation stages, generally using a petroleum pitch. Finally, the product is graphitised at 2500°C to 3000°C to obtain the hexagonal crystalline structure that is characteristic of graphite. Graphitisation is carried out using cleaning agents such as NaF, MgF2 or Cl2 to obtain high-purity nuclear graphite. This type of treatment, however, probably accounts for the presence of chlorine in the graphite, which will lead to the formation and capture of 36Cl in the graphite used in gas-cooled reactors.

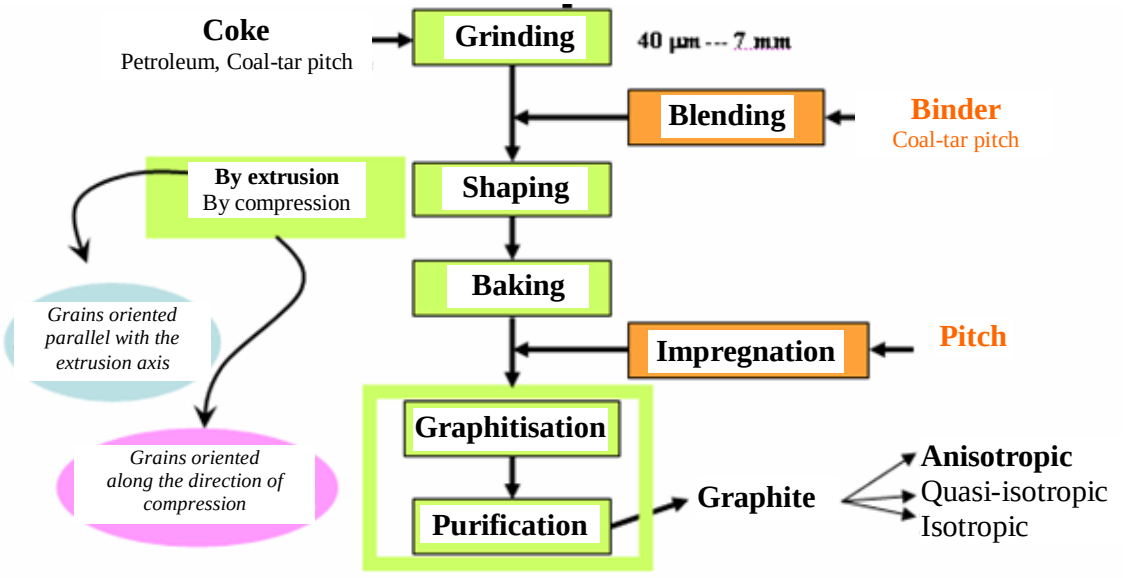

Figure 5 – Nuclear graphite manufacturing process (by courtesy of Jean-Pierre Bonal, see C.E. Vaudey's thesis)

3 Carbon and graphite characterisation

Several investigation techniques were used for the purposes of this study to obtain quantitative data on different scales (nanometric to micrometric). A brief description of the

three main techniques used for this work – namely transmission electron microscopy, Raman microspectrometry and X-ray diffraction – is given below.

3.1 High-resolution transmission electron microscopy

Transmission electron microscopy (or TEM) is a microscopy technique in which an electron beam is 'transmitted' through an ultra-thin sample (Figure 6). The incident electrons interact with the sample, giving rise to the scattered electron beams that form the image. In lattice fringe mode, the resolution of the images obtained can be as high as 0.14 mm in the case of the Jeol 2011 TEM used for this work. This part of the report is not intended as a course in TEM and its carbon-related applications. Those interested in further reading can refer to Agnès Oberlin's impressive paper [2], which is a 'bible' for novices in TEM and carbons, as well as to the articles by Rouzaud et al. [1-3].

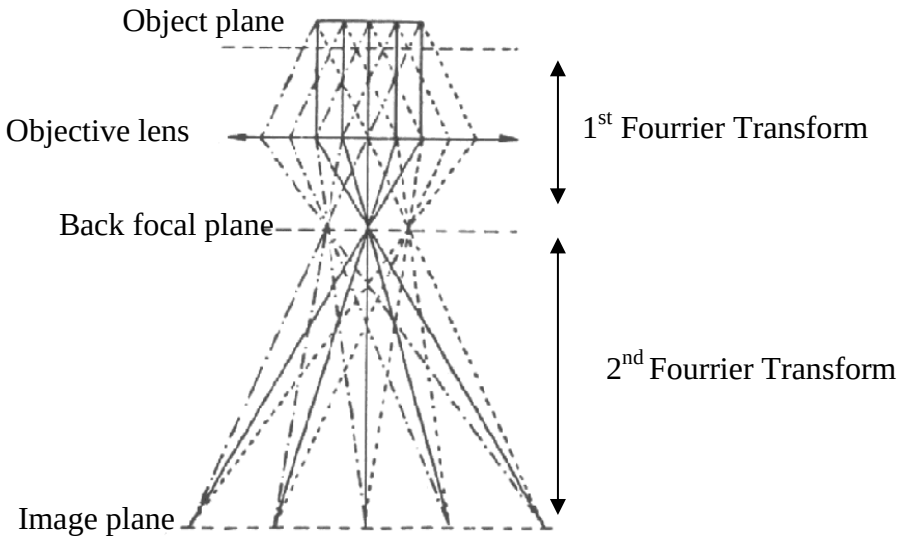

Figure 6 – Electron beam path in the objective lens of the TEM

For the most part, two TEM modes were used for this work:

- '002 lattice fringe mode', often somewhat improperly referred to as 'high-resolution' transmission electron microscopy or HRTEM; this mode involves the use of a phase contrast (interference between beams diffracted by the graphene layers, and the directly transmitted 000 beam). Each fringe allows direct observation of the profile of

the aromatic layers (i.e. the graphene layers), with a resolution better than 0.2 nm. The example of graphite is shown in Figure 7 below and in Figure 4 earlier in the document, which illustrates the graphitisation of a graphitisable carbon.

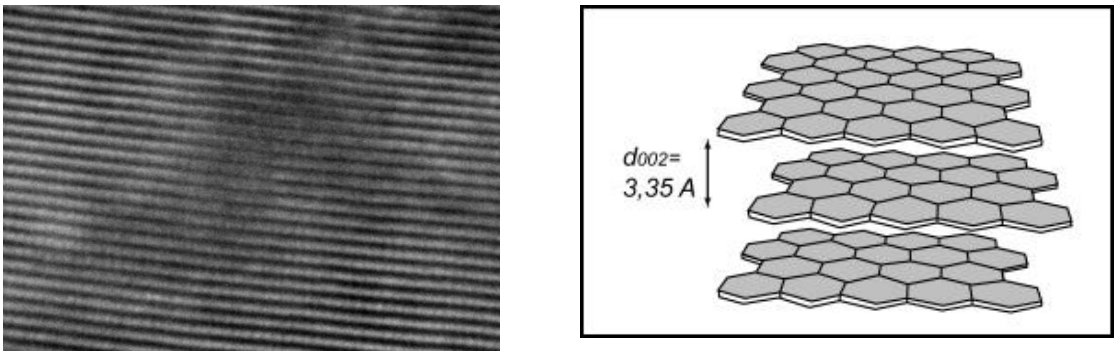

Figure 7 – Right: TEM image of nuclear graphite in 002 lattice fringe mode (the black fringes represent the profile of the graphene layers and are spaced of 0.336 nm; Left: Structural sketch

- 11 dark field mode, which makes it possible to observe graphite crystallites through the rotational moiré patterns they form when stacked. This involves amplitude contrast: the image is produced by 11(0) diffracted beams selected by a small diaphragm inserted in the focal plane of the objective lens, where the diffraction pattern is formed. By this mode, resolution is about 1 nm. Figure 8 shows an example of graphite crystallites observed by 11 dark field mode. The different images were obtained by varying the orientation of the objective diaphragm on the 11(0) diffraction ring (and, therefore, the orientation of the moiré fringes).

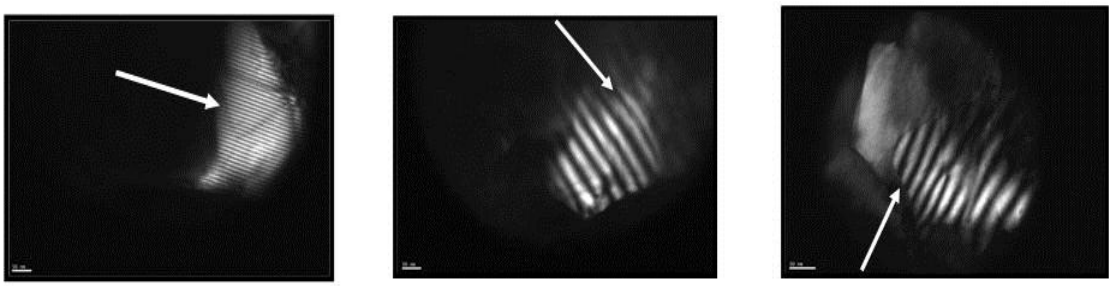

Figure 8 – Graphite crystallites seen under the TEM (by 11 dark field mode); different crystallites can be observed by varying diaphragm orientation. The scale bar is 10 nm.

3.2 Raman microspectrometry

Raman microspectrometry is a non-destructive optical method used to study the vibrational (rotational for gases) and structural properties of a solid, liquid or gaseous material. This technique is characterised by its high spatial resolution (approx. 1 µm) and complements infrared spectroscopy. It involves focusing a beam of monochromatic light onto a sample (an illuminated surface no more than 1 µm in diameter) and analysing the scattered light, which includes both the energy of the exciting light (Rayleigh line) and other energies characteristic of the vibrational signature of the medium (Stokes and anti-Stokes lines) (Figure 9). A Raman system is equipped with a laser, used as an exciting source (for example, an Argon laser: λ=514.5 nm in the case discussed here), and a spectrometer equipped with two diffraction gratings: one is a low-dispersion grating (1800 lines/mm) used for highly sensitive analysis, the other is more dispersive (3000 lines/mm) and used for analysis with high spectral resolution.

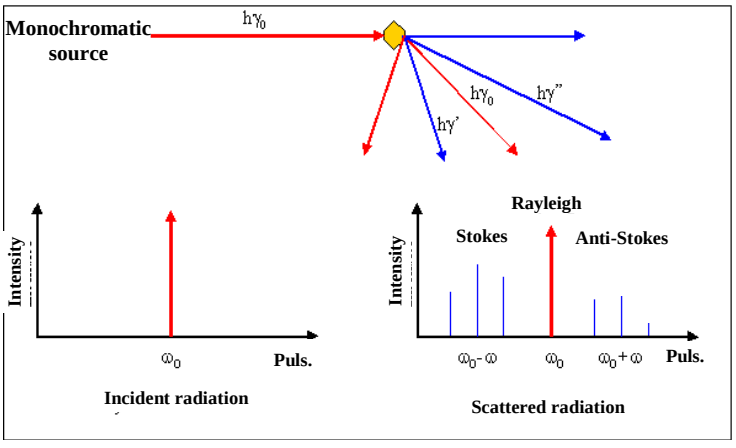

Figure 9 – Principle of Raman scattering

Monocrystalline graphite, such as highly oriented pyrolytic graphite (HOPG), belongs to space group $P6_3/mmc$. The symmetry properties of the normal optical mode of the unit cell (4 atoms, symmetry D_{6h}^4), at the centre Γ of the Brillouin zone, are described by Tuinstra and Koenig [4]:

$$\Gamma_{vib} = 2B_{2g} + 2E_{2g} + A_{2u} + E_{1u}$$

The only fundamental Raman-active modes are the two E_{2g} modes, while the A_{2u} and E_{1u} modes are infrared-active.

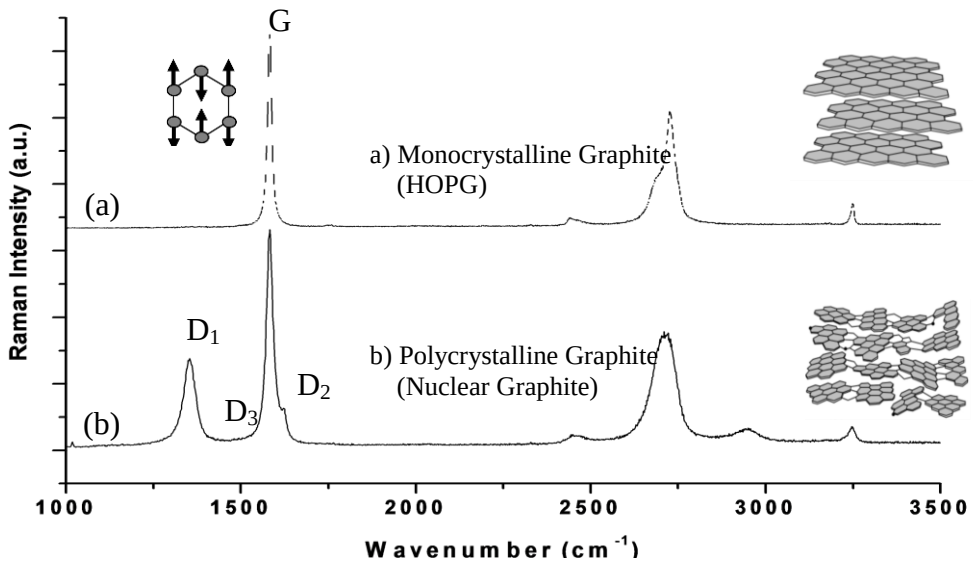

Figure 10 – Raman spectra of a) an highly oriented pyrolytic graphite (HOPG), which is a monocrystalline graphite, in comparison with b) a disordered graphitic carbon

The first Raman-active mode represents shear vibrations and occurs at low frequency (~42 cm^{-1}). Its frequency is close to Rayleigh scattering which makes it very hard to observe. The second is a deformation mode of the cycle in the plane, with a frequency in the region of 1580 cm^{-1}, called the G band (Figure 10a). Other, second-order, bands appear, which correspond to harmonic and/or combination modes.

The Raman spectrum of the graphite undergoes a significant change in the case of a disordered graphitic carbon, with the appearance of disorder (structural defects that limit the extent of the crystallites and stacking perfection (Figure 10b). New bands are detected, the most significant of which are the bands called D_1 (close to 1360 cm^{-1}) and D_2 (close to 1620 cm^{-1}). The intensity of the defect bands increases with respect to the G band as the disorder in the graphite structure increases. A significant amount of research has been devoted to these signatures, which were discovered in the early 1970s. They are hard to interpret and it is

possible that the physical mechanisms behind their activation have yet to be fully elucidated. The D_1 band was initially interpreted by Tuinstra and Koenig by an A_{1g} symmetry mode that becomes active in Raman spectrometry as a result of the limited size of the crystallites. Unfortunately, this theory does not explain the dispersive nature of the D_1 band, illustrated by the fact that its position and intensity depend on exciting photon energy (Figure 11). Other authors have recently attributed this dispersive nature to a double-resonance phenomenon [5].

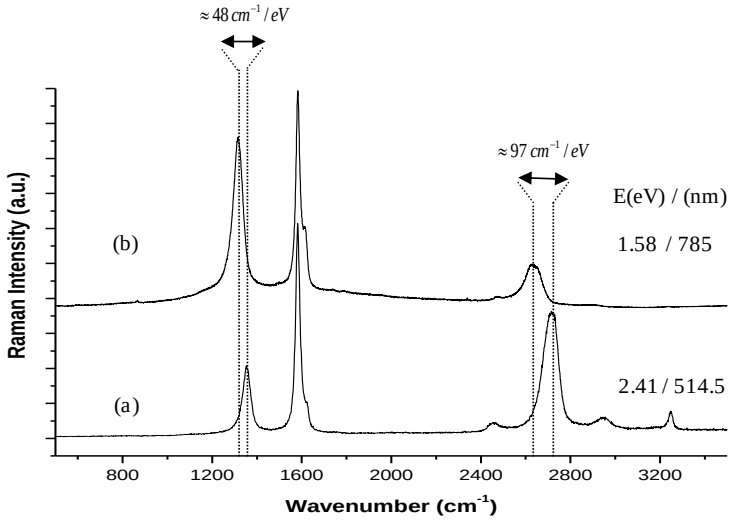

Figure 11 – First- and second-order Raman spectra of nuclear graphite obtained using two excitation energies: 1.58 eV and 2.41 eV

Tuinstra and Koenig proposed an empirical relation – in quantitative terms – between the D_1/G intensity ratio and crystallite diameter, L_a, (based on XRD calculations):

$$\mathbf{La = C(\lambda) / (I_{D1}/I_G)} \text{ where } C(\lambda) = 4.4 \text{ nm if } \lambda = 514.5 \text{ nm.}$$

This calibration was completed by Ferrari and Robertson *(*A.C. Ferrari, J. Robertson, Phys. Rev. B 61 (2000) 14095) for highly disordered (right side of the curve), and amorphous (left side), carbons (Figure 12).

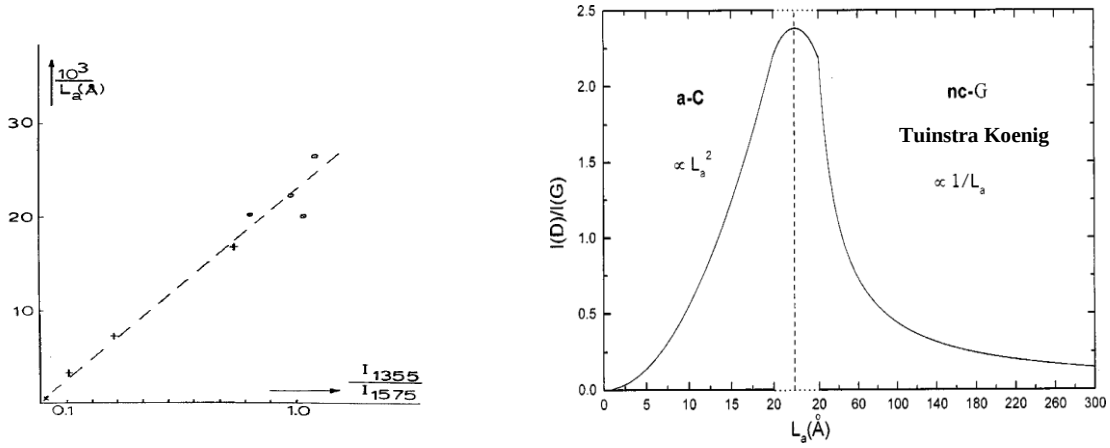

Figure 12 – Calibrations between intensity ratio and crystallite size (on the left : Tuinstra & Koenig relation, on the right : Ferrari & Roberston relation)

The D_2 band appears to be as a shoulder of the G band, although its significance is still not clear. It is thought that it might be caused by a spacing distribution between the graphene layers.

For the most highly disordered carbons, such as soots and activated carbons, spectrum intensity does not generally return to the baseline between the G and D_1 bands. Spectral decomposition is considerably improved by introducing a supplementary contribution centred around 1540 cm^{-1}. The origin of this band, referred to as D_3 here, remains the subject of considerable debate. It could be due to sp^3 carbons located at the edges of aromatic layers (sp^2 carbons) [3].

The D_2 band appears to be as a shoulder of the G band, although its significance is still not clear. It is thought that it might be caused by a spacing distribution between the graphene layers.

For the most highly disordered carbons, such as soots and activated carbons, spectrum intensity does not generally return to the baseline between the G and D_1 bands. Spectral decomposition is considerably improved by introducing a supplementary contribution centred around 1540 cm^{-1}. The origin of this band, referred to as D_3 here, remains the subject of considerable debate. It could be due to sp^3 carbons located at the edges of aromatic layers (sp^2 carbons) [3].

3.3 X-ray diffraction

The crystalline state is characterised by the tri-periodic distribution of an atomic cell in space. This ordered atom distribution forms parallel, equidistant planes, known as hkl lattice planes. Inter-lattice spacings are in the region of 0.15 Å - 15 Å and depend on the arrangement and diameter of atoms in the crystal lattice. They are constant and characteristic of the crystal and can be calculated by X-ray diffraction. A monochromatic, parallel X-ray beam is diffracted by a crystal in a given direction by each family of lattice planes whenever **Bragg's law** or condition is satisfied (Figure 13):

$$n\lambda = 2d \sin \theta$$

where n = the diffraction order

λ = the wavelength of the X-ray beam,

d = the spacing between two successive lattice planes,

θ = the X-ray incident angle.

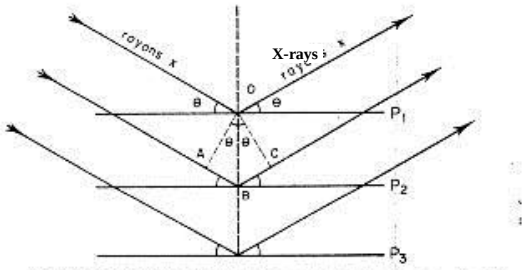

- X-ray diffraction by a family of lattice planes.
P1. P2. P3. etc. are the planes of this family; 0 is the Bragg angle.

Figure 13 – X-ray diffraction by a family of lattice planes

The full width at half maximum values of 002 and 110 reflections (see Figure 14) respectively give the average heights and diameters, L_c and L_a, of the coherent domains (improperly referred to as 'crystallites') using the Debye Scherrer formula:

$$L_{a,c}=K\lambda/\beta\cos\theta$$ where K= 0.89 for L_c (002) and 1.84 for L_a (110) **[6]**.

In order to subtract instrumental broadening, the parameter β was corrected using the equation $\beta = \sqrt{\beta_g^2 - \beta_{GGG}^2}$ where β_g is the full width at half maximum of the measured peak, and β_{GGG} is the FWHM of the standard sample made of very large crystals, in this case a gadolinium-gallium garnet (GGG) -$Gd_3Ga_5O_{12}$-, obtained experimentally.

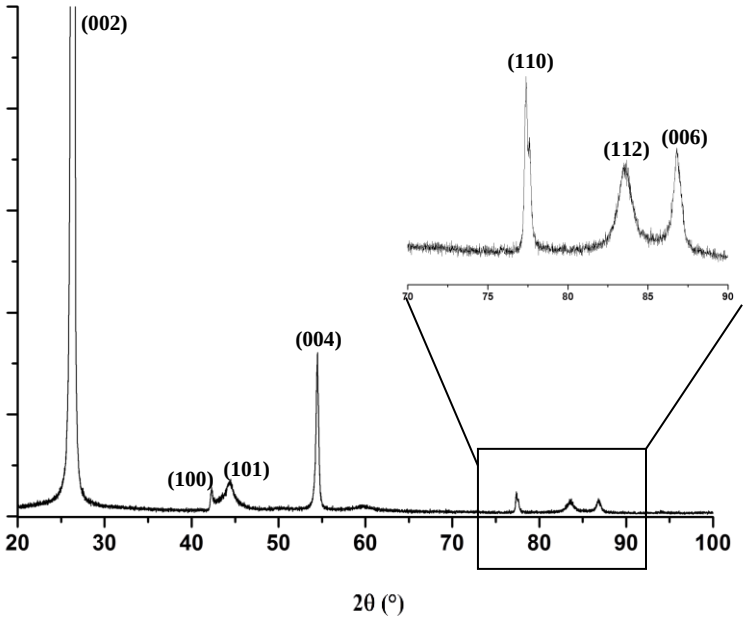

Figure 14 – Example of a diffraction pattern for SLA2 nuclear graphite

4 Characterisation of virgin nuclear graphite

4.1 Study of the nuclear graphite manufacturing process

Anthracene-based coke was used as a benchmark for monitoring the nuclear graphite manufacturing process as a function of temperature. This pure, uniform homogeneous reference carbon has been used for fifty years by GFEC, the French Carbon Group. It is one of the most graphitisable carbons and a highly satisfactory analogue of petroleum cokes, the predominant component making up nuclear graphites. During the first stage of the process, the anthracene molecule ($C_{14}H_{10}$) undergoes pyrolysis at a temperature of 450°C and a pressure of 0.2 MPa under argon for one hour to produce a semi-coke. The material is then heated to various temperatures ranging from 1000°C to 2900°C.

In the X-ray diffraction pattern in Figure 15, the largest contribution comes from the 002 reflection around 2θ =26°. This is due to the preferential orientation of the lamellar coke grains (or flakes).

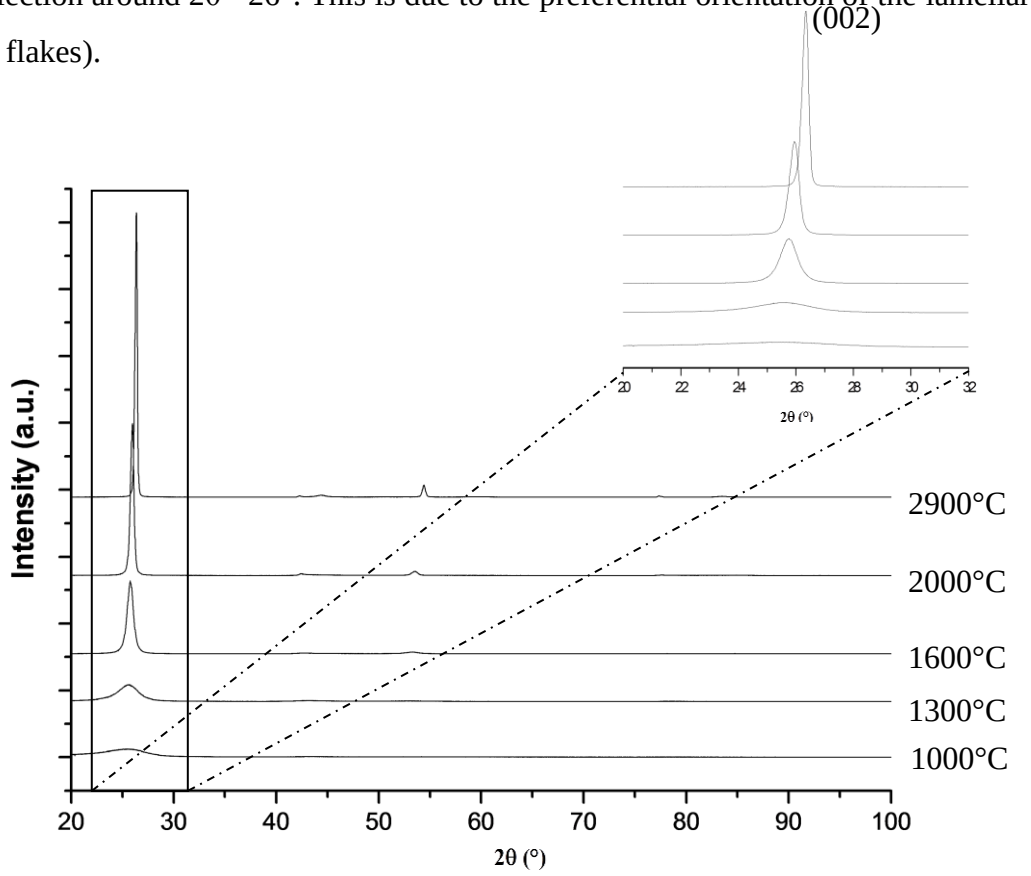

Figure 15 – X-ray diffraction pattern for an anthracene semi-coke annealed at various temperatures up to 2900°C

As the temperature rises, the 002 reflection becomes increasingly narrow and shifts towards the wide angles, reaching 26.4°2θ in the case of pyrolysis at 2900°C. These two phenomena respectively indicate increased crystallite size and a significant decrease in inter-layer spacing (d_{002} falling from around 0.35 nm at 1000°C to about 0.336 nm, although not as low as the value observed in graphite, which is 0.3354 nm).

The temperature-related growth of coherent domains (‘crystallites’) can also be observed through the transmission electron microscope in 11 dark field mode (see Figure 16). Each stack placed on the Bragg angle lights up, making it possible to evaluate – by default – the diameter of the crystallites by measuring the moiré patterns they form when they are superimposed on one another.

a)

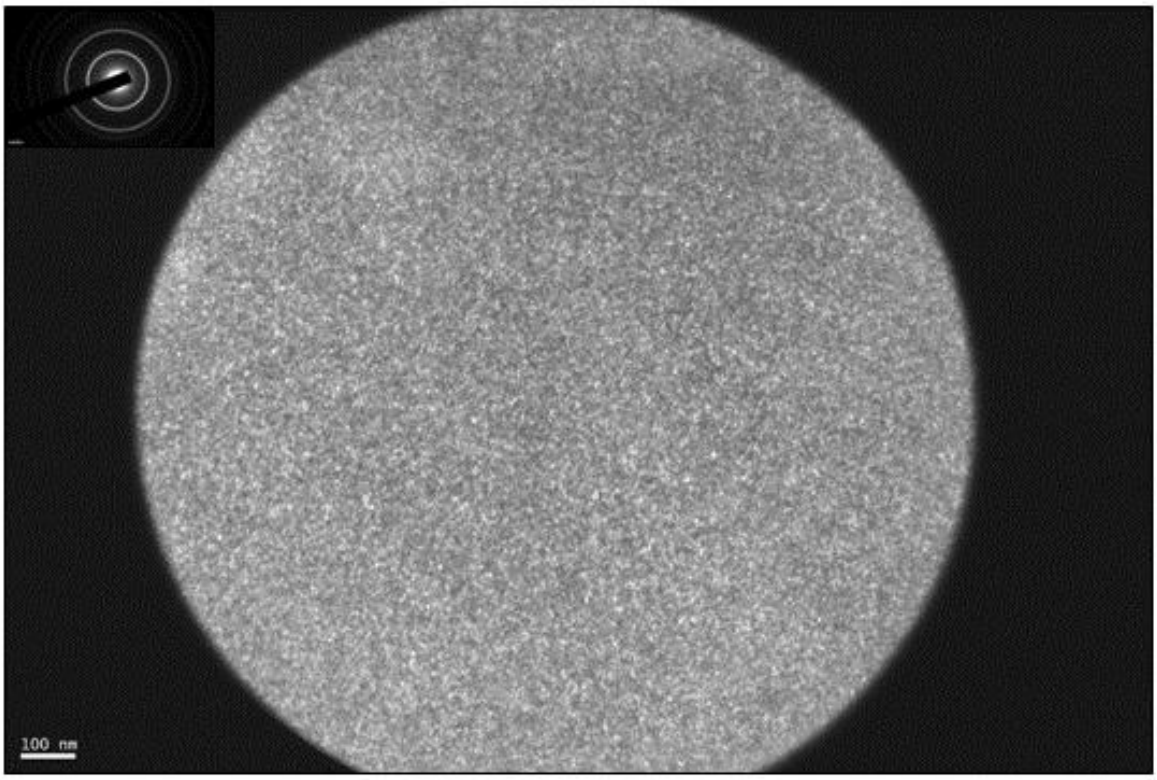

b)

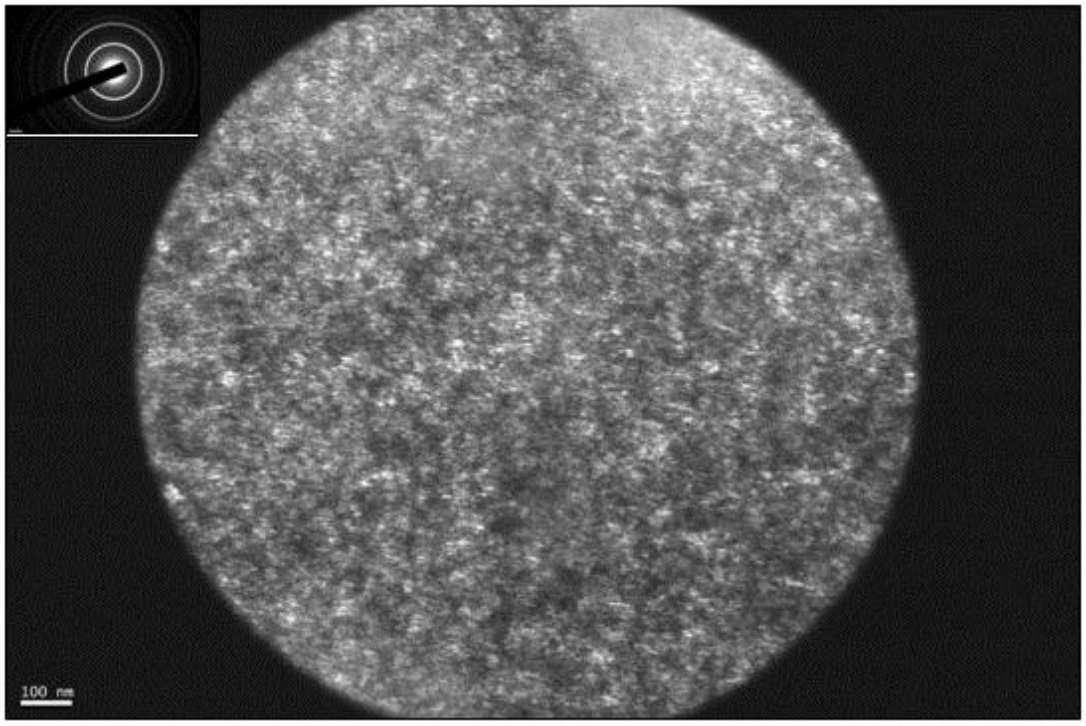

c)

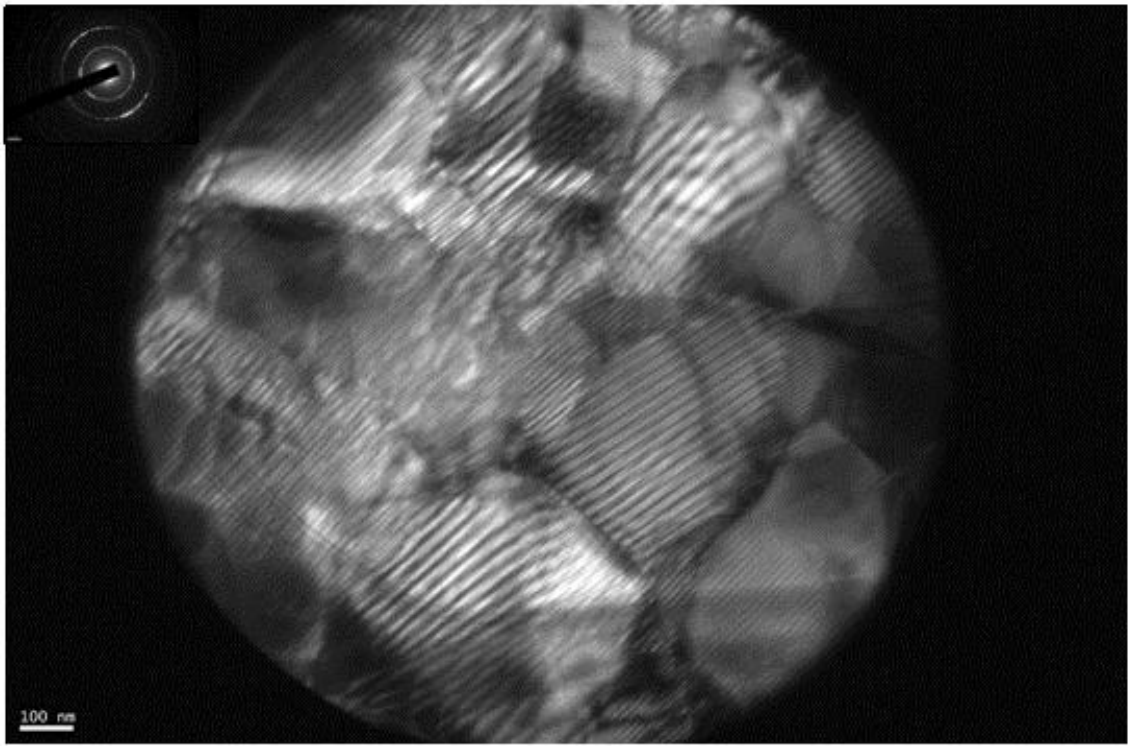

Figure 16 – 11 dark field image of an anthracene-based coke annealed at various temperatures: a) 1600°C; the inset SAED diagrams illustrate the increased degree of graphitisation: at 1600°C, as shown here, the hk rings remain broad and faint.

Spectroscopic analysis provides particularly complementary structural information. This is especially true of Raman microspectrometry, a technique that is highly sensitive to this structural improvement. It is easy to use for quantitative studies, provided, of course, suitable precautions are taken regarding wavelength, polarisation and power of the exciting light.

Figure 17 shows typical variations in Raman spectra as a function of annealing temperature in the anthracene-based semi-coke obtained at 450°C.

First, the G and D_1 bands were seen to be finer as annealing temperatures increased to 1600°C, the temperature at which the D_2 band began to be distinguishable from the G band.

Next, the intensity of the D_1 and D_2 bands decreased gradually and significantly with respect to that of the G band due to to the graphitisation phenomenon.

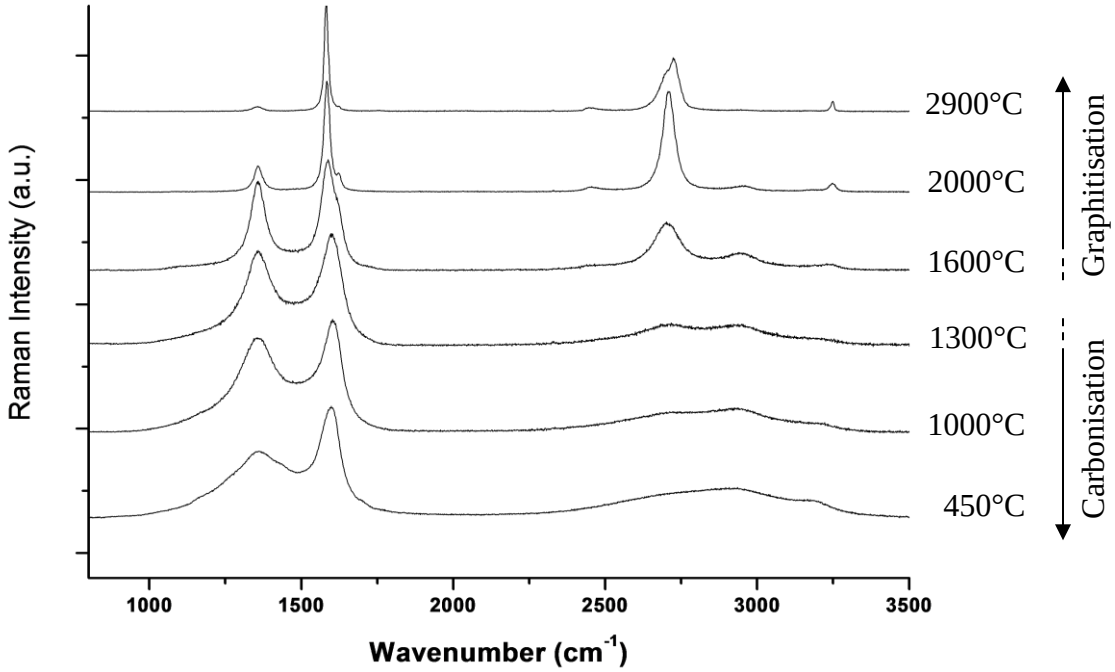

Figure 17 – Variations in Raman spectra for anthracene-based cokes as a function of annealing temperature up to 2900°C, using a 514.5 nm laser excitation wavelength

Spectral decomposition was achieved using conventional adjustment procedures and the Renishaw Wire 2.0 program. This yielded the following parameters: position, intensity, FWHM and the integrated intensity (i.e. the surface area) for all bands (D_1, D_2, D_3 and G). Figure 18 shows a first-order deconvolution.

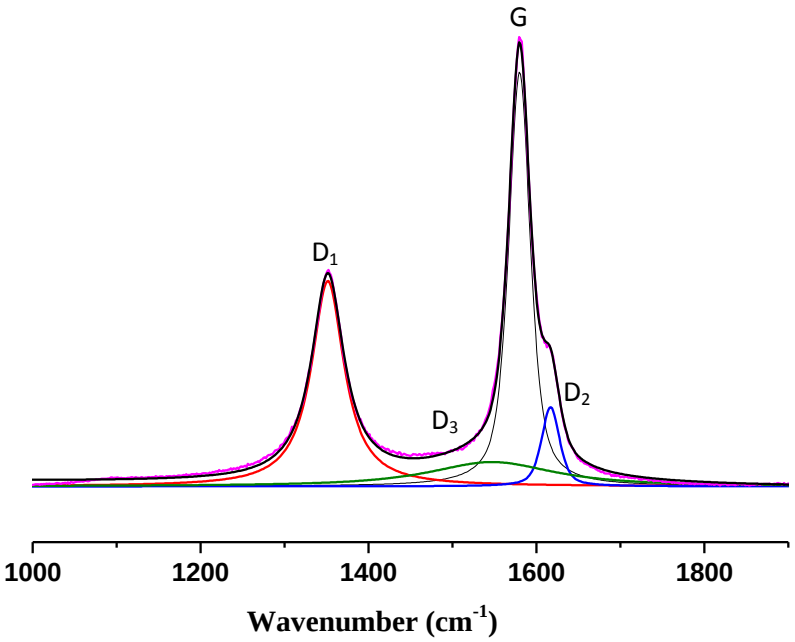

Figure 18 – First-order Raman spectrum decomposition for an anthracene-based coke heated to 1900°C.

As part of the quantitative aspect of this research work, first-order Raman spectra were adjusted to observe temperature-related changes in what seemed to be the two most promising parameters, namely the intensity ratio $\frac{I_{D_1}}{I_G}$ and the full width at half maximum of the G vibrational band ($FWHM_G$). Measurement uncertainty was determined using ten Raman spectra for each sample. It should be stressed, however, that the intensity ratio measured by adjusting the spectra discussed here differs from that calculated by Tuinstra and Koenig, which was obtained by simply determining the band height of the raw spectra. Figure 19 shows that both parameters clearly follow the same pattern as a function of temperature, with a sharp falling from 2400°C, temperature at which the structure tends towards the graphite structure.

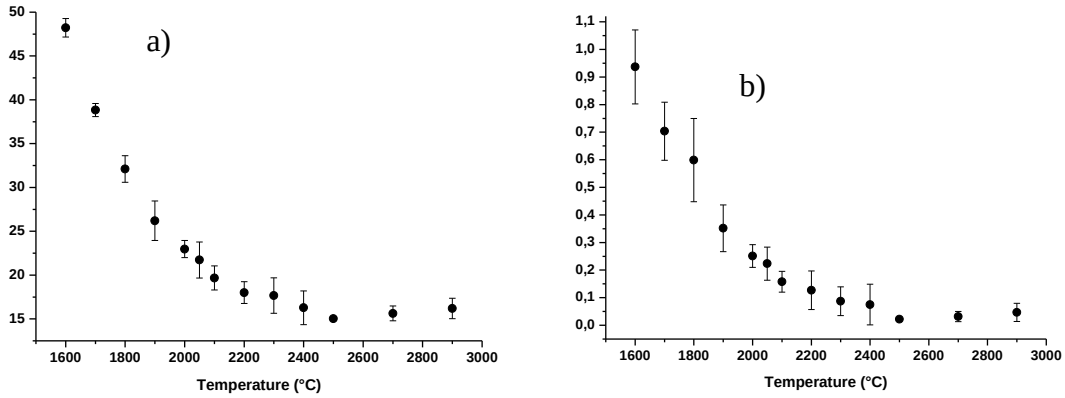

Figure 19 – Results of Raman spectrum decomposition as a function of annealing temperature: a) D1 to G intensity ratio; b) full width at half maximum of the G band.

As expected, the full width half maximum of the G band increase linearly according to the intensity ratio $\frac{I_{D_1}}{I_G}$ displays linear behaviour for various temperatures of treatment (Figure 20). This correlation is expressed as follows:

$$\mathbf{FWHM_{G\ band} = 14 + 35\ \frac{I_{D_1}}{I_G}\quad (R^2 = 0.99)}$$

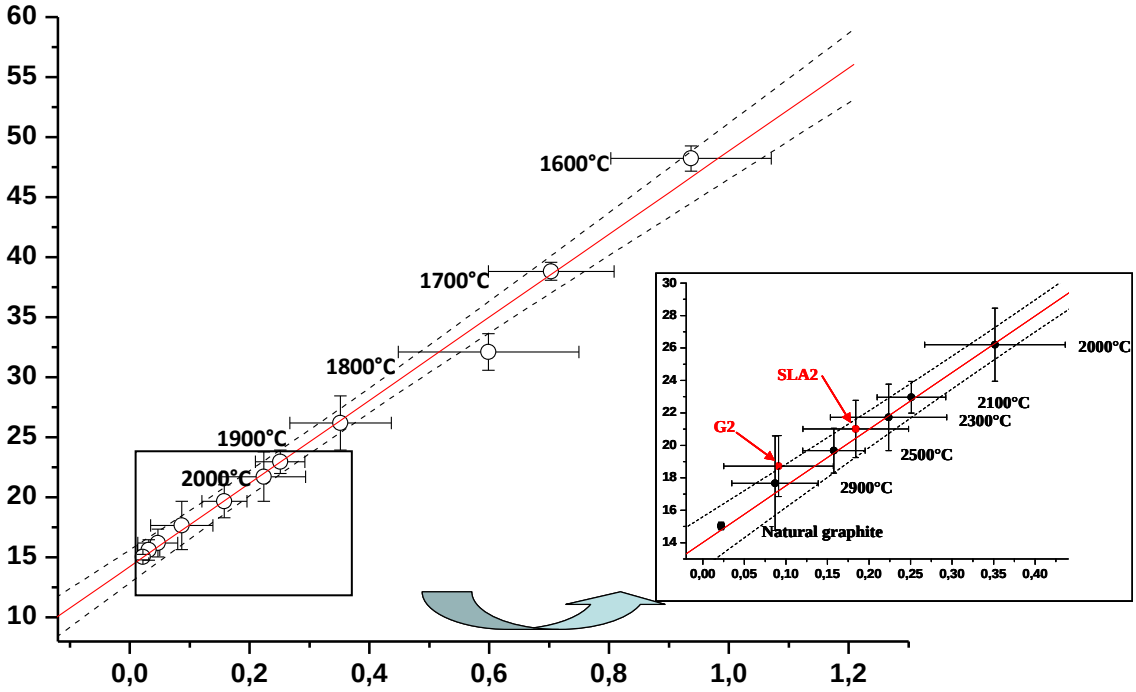

Figure 20 – Changes in the full width at half maximum of the G band as a function of the D1/G intensity ratio for an anthracene-based coke subjected to various temperatures of treatment

The virgin nuclear graphites used at the Saint Laurent A2 (SLA2) and Marcoule G2 nuclear reactors are located in the domain of the most graphitised carbons and are perfectly positioned on the correlation line. This curve can thus be used to classify these graphitised materials according to the degree of graphitisation. It can be clearly seen that G2 nuclear graphite is more graphitised than SLA2.

This result, obtained using Raman microspectrometry, was confirmed by XRD measurements and, in particular, by determining the sizes of crystallites (L_c and L_a) from the full width at half maximum values of diffraction peaks 002 and 110 respectively (see page 15). For comparison, these structural parameters were also measured for the main nuclear graphites: a petroleum coke, representative of a 'nuclear-grade' petroleum coke, and a coal-tar pitch coke

similar to that used to make nuclear graphite. Table 1 gathers all the parameters calculated from XRD patterns (L_c, L_a) and those determined by Raman microspectrometry.

SAMPLE	L_C (NM) XRD (002)	L_A (NM) XRD (110)	$\frac{I_{D_1}}{I_G}$	$FWHM_G$ (CM^{-1})
Natural graphite (Ceylon)	54.4	169.1	0.009±0.008	15.38 ± 1.17
Petroleum coke (MOT) (2800°C)	29.3	92.3	0.040±0.010	17.05± 1.29
Pitch coke (LPC) (2800°C)	28.4	78.1	0.095± 0.034	19.53 ± 1.86
Nuclear graphite (G2)	41.3	112.0	0.09±0.06	19.32 ± 1.87
Nuclear graphite (SLA2)	29.4	81.0	0.180±0.060	21.01 ± 1.76

Table 1 - Parameters calculated (Lc, La) from XRD patterns and measured by Raman microspectrometry ($\frac{I_{D_1}}{I_G}$, FWHMG) for different types of graphite

In the case of natural graphite, petroleum coke and pitch coke, a good correlation can be seen between the parameters obtained by XRD measurements and those obtained by Raman microspectrometry: the smaller the crystallites, the higher the intensity ratio and full width at half maximum of the G band. This is also true for the two nuclear graphites, G2 and SLA2. Nonetheless, as already observed in other studies, the Raman La values seem significantly higher than those calculated from XRD patterns. Furthermore, the intensity of the D_1 defect band of the SLA2 nuclear graphite should be no higher than that of the pitch coke annealed at 2800°C: this is not the case. This behaviour, which has also been observed on earlier occasions, is probably due to the fact that the pitch is less completely graphitised when inserted between the coke flakes.

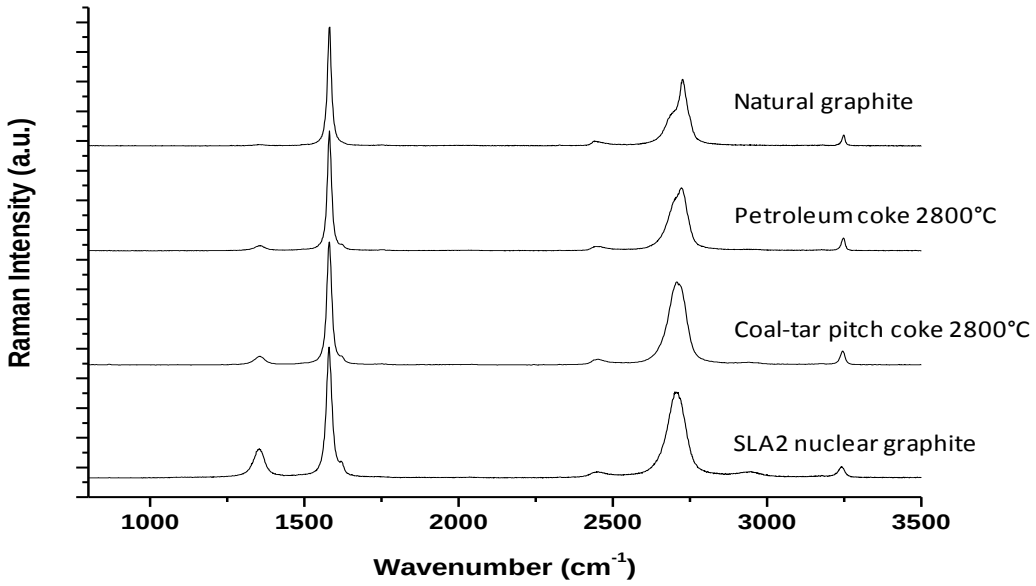

Figure 21 – Comparison of Raman spectra for various types of carbon; from the top to the bottom : natural graphite, petroleum coke heated at 2800°C, coal tar pitch coke heated at 2800°C, SLA2 nuclear graphite

This variation could also be explained by the polarisation of the exciting light and the orientation of the crystallites making up nuclear graphite. The laser excitation beam causes the polarisation in the sample to be parallel to the incident electric field. For perfectly symmetrical vibration, the scattered Raman light maintains the same polarisation as the incident light. It can be concluded from this that the Raman intensity observed strongly depends on the direction of observation. Our work shows that this aspect can serve as a parameter for characterising the orientation of the crystallites making up nuclear graphite.

Figure 22 shows the Raman spectra obtained on the basal plane and at the edge of an HOPG monocrystal, with the laser beam polarised parallel with and perpendicular to the graphene layers. The intensity ratio of the E_{2g} vibrational band is almost 100% on a basal plane (isotropic section), but only 10% for the edge (it should be equal to zero if the graphene layers were all exactly orthogonal to the polarisation direction). In nuclear graphite, however, the intensity ratio of the E_{2g} band can reach 80% (see Figure 22b). This result proves that nuclear graphite is made up of small crystallites whose orientation is random, to varying degrees, on the area covered by the laser spot. A schematic illustration of these crystallites can be seen below.

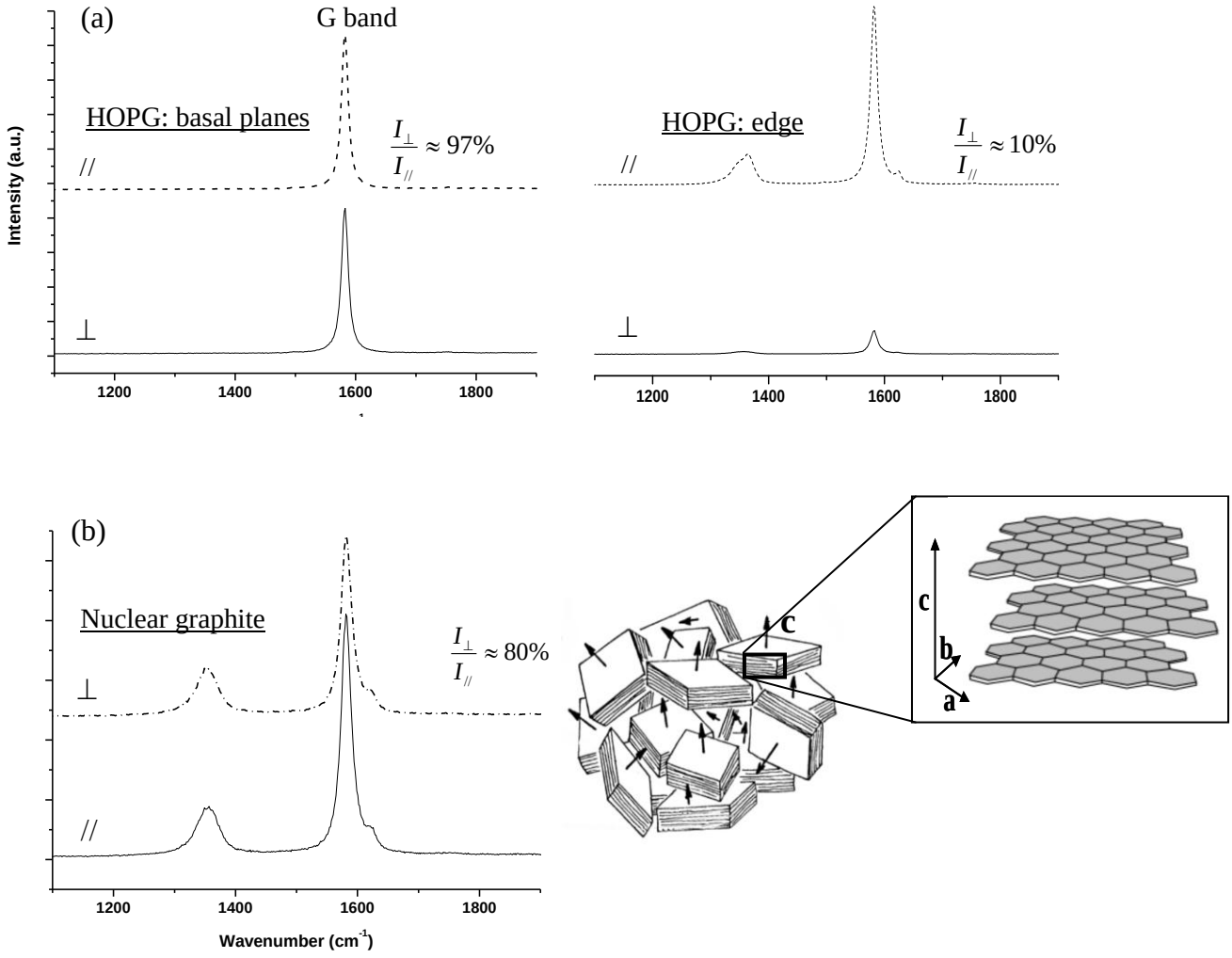

Figure 22 – Laser beam polarisation effect on Raman spectra. Effect of the random orientation of the crystallites making up nuclear graphite, leading to a decreased I -/ I // ratio in the G band and, consequently, to an increased D1/G ratio

Such more or less random orientation of crystallites can lead to a virtual increase in the defect band owing to the decrease in the G band. To minimise this effect when measuring the degree of graphitisation, circular polarisation was always adopted for our studies.

Our Raman results were confirmed by XRD diffractograms recorded for a sample placed normally to the incident beam (Figure 23). The diffraction pattern reveals the existence of all possible graphite reflections, in particular 001 (002, 004, 006) strong reflections. This confirms that arrangement of crystallites in the block of nuclear graphite is not exactly parallel to the flakes but is more or less random which allows these planes to be on the Bragg angle.

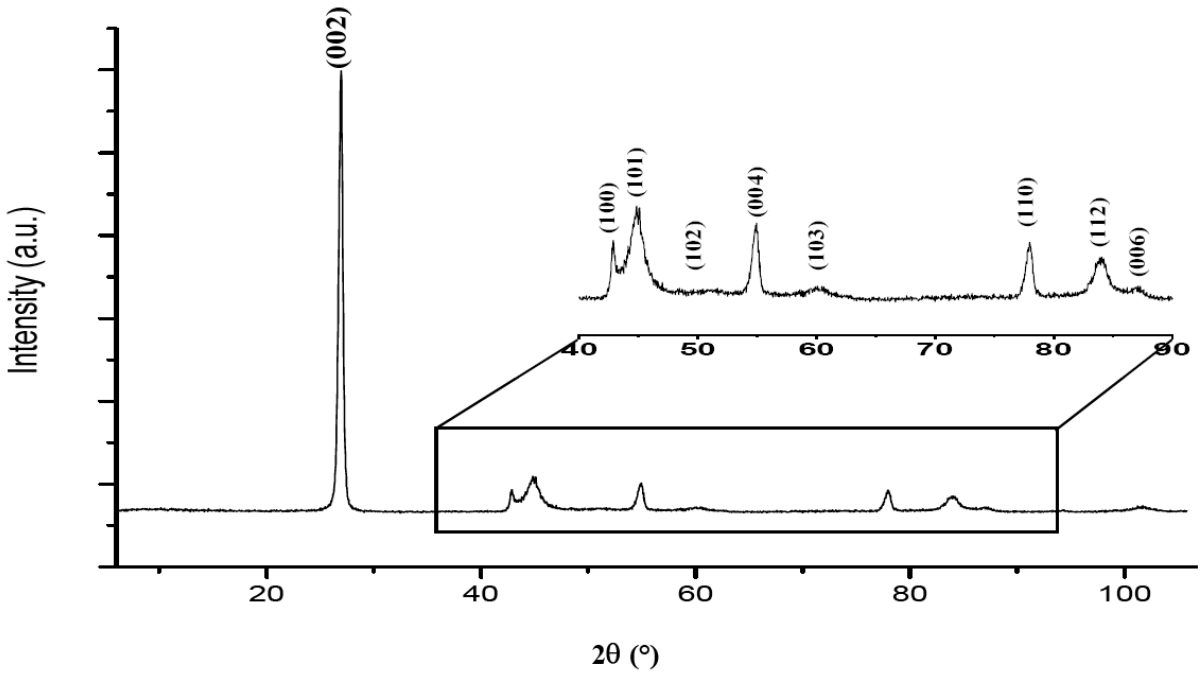

Figure 23 – X-ray diffraction pattern for SLA2 nuclear graphite

Following on Tuinstra and Koenig, Beyssac et al. proposed using the structural parameter R_2 to characterise the degree of organisation of carbonaceous materials (metamorphosed coals, cokes and anthracites graphitised to varying degrees).

$$R_2 = \frac{A_{D_1}}{(A_G + A_{D_1} + A_{D_2})}$$ where A is the area of the band

Figure 24 shows two Raman maps, acquired in point-to-point scanning mode, of two samples of SLA2 virgin nuclear graphite. The images highlight the dispersion in R_2 values and, therefore, in the intensity of the Raman defect bands. Two main conclusions can be drawn from this. First, R_2 varies from 0.25 to 0.35 over most of the area analysed, this variation probably being related to the disorientation of the crystallites making up the nuclear graphite. Second, this parameter is significantly lower (less than 0.1) in certain specific areas.

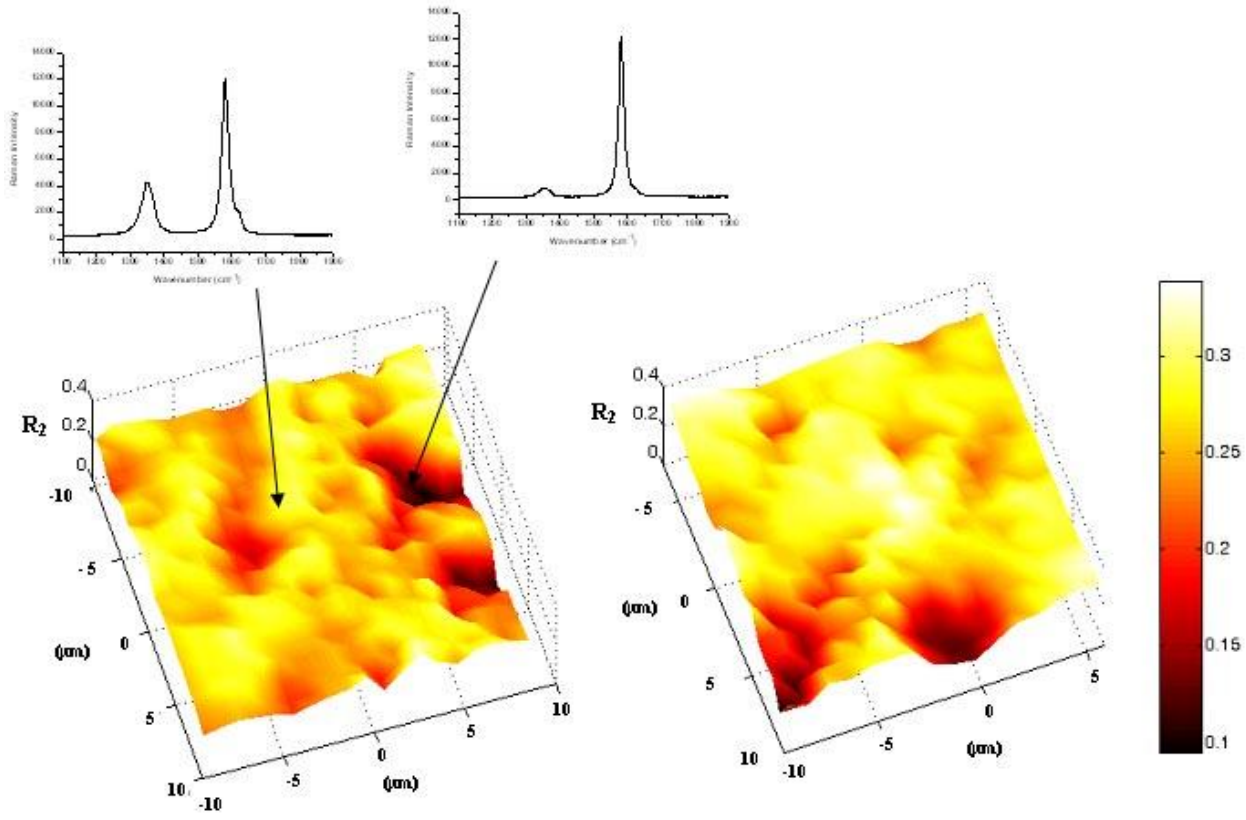

Figure 24 – Raman maps showing variations in the structural parameter R2 at the micrometric scale in nuclear graphite

This variation reflects micrometric-scale heterogeneity in the degree of organisation of the nuclear graphite. The sharp local decrease in the defect band is probably related to how the nuclear graphite is manufactured and, therefore, to its composition. Nuclear graphite is made up of two main elements: a granular petroleum coke, which represents by far the larger proportion, and a binder consisting of coal-tar pitch. The two elements are mixed together, then heated to 2800°C. Petroleum coke is generally regarded as the more graphitisable of the two

components, which could account for the significant decrease in the defect bands in the Raman spectrum of the nuclear graphite as a whole.

Micrometric-scale observation under the optical polarising microscope

The texture of nuclear graphite was examined under a LEICA DM RXP optical polarising microscope. Observations were carried out in reflection mode, between crossed polariser and analyser, with an accessory wave plate – also known as a 'gypsum plate' or 'sensitive tint plate' – inserted. The purpose of this wave plate was to introduce an additional path difference between the ordinary and extraordinary rays and, therefore, an additional phase shift to that induced by the nuclear graphite crystals under observation. Under these conditions, the interference colours of the anisotropic domains are yellow or blue, while the isotropic parts are magenta. Note that this type of observation mode requires carefully polished sections.

In Figure 25, these nuclear graphites clearly appear as carbon-carbon composites. The grains or flakes of petroleum coke, characterised by large, optically anisotropic domains can be clearly distinguished (two are encircled by a dotted line in the image on the right), separated by the coal-tar pitch binder. The binder is characterised by small isochromatic domains and, more particularly, a considerable porosity, a characteristic initially attributed to volatile molecules during the nuclear graphite manufacturing process (highest temperature of treatment between 2500°C and 3000°C).

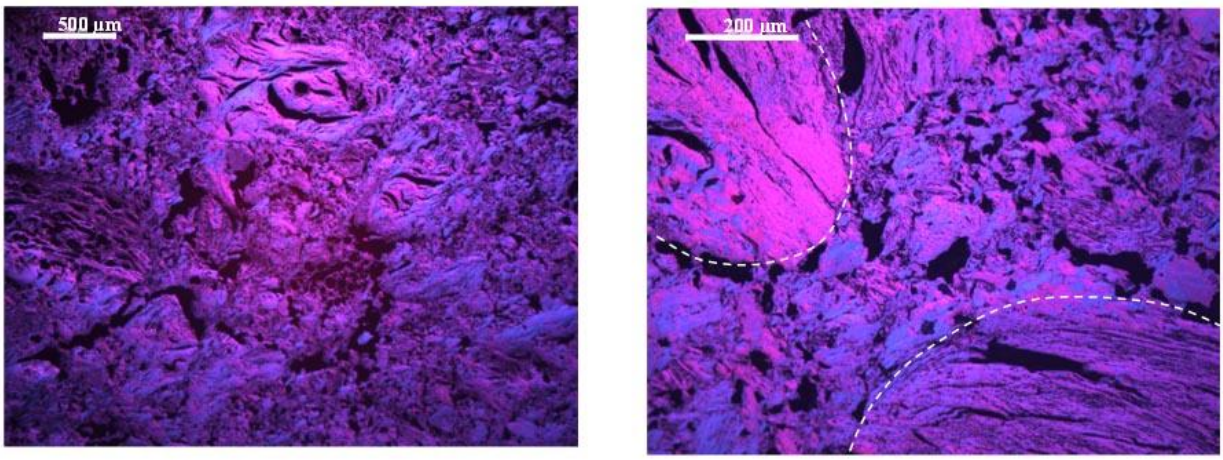

Figure 25 – Images observed under the optical microscope in polarised light showing the different components making up nuclear graphites, which clearly appear as carbon-carbon composites

Micrometric to nanometric observation under the transmission electron microscope

In order to observe nuclear graphite under the transmission electron microscope on a nanometric scale, the bulk material must be made thin enough to achieve electron transparency. Several methods can be used for this purpose. The simplest is to reduce the size of the graphite fragments by grinding a small amount of material in a mortar under alcohol. The resulting suspension then undergoes ultrasonic treatment and a drop is placed on a holey grid and dried. The finest grains (generally lamellae), positioned so that they form a bridge between the edges of the holes, can thus be directly observed under optimum conditions (nanometric thickness limiting image overlap superimposition, no amorphous membrane to induce background noise that is particularly problematic when characterising the most disordered carbons). The lamellar structure of the nuclear graphite can be clearly seen in Figures 26 and 27. The dark rectangles visible in the folds of the lamellae are stacks of polyaromatic layers (graphene layers) exactly placed on the Bragg angle. The shape and size of the rectangles show that the layers are large and perfectly plane.

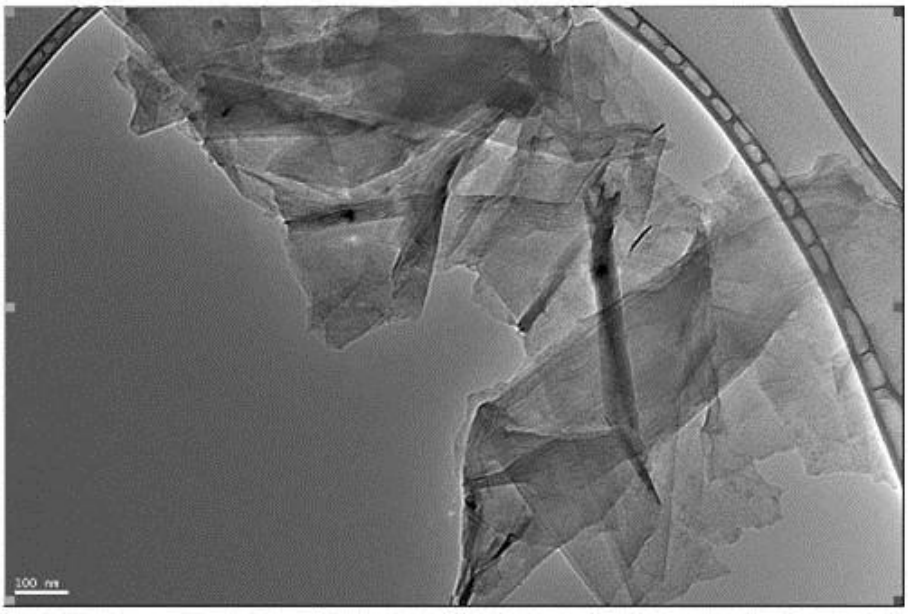

Figure 26 – TEM images (Bright Field mode) on a submicron scale showing the lamellar structure of SLA2 nuclear graphite. The darker bands are folds. The graphene layers are placed below the Bragg angle in these folds and can thus be observed directly in 'high resolution' mode (see Figure 27).

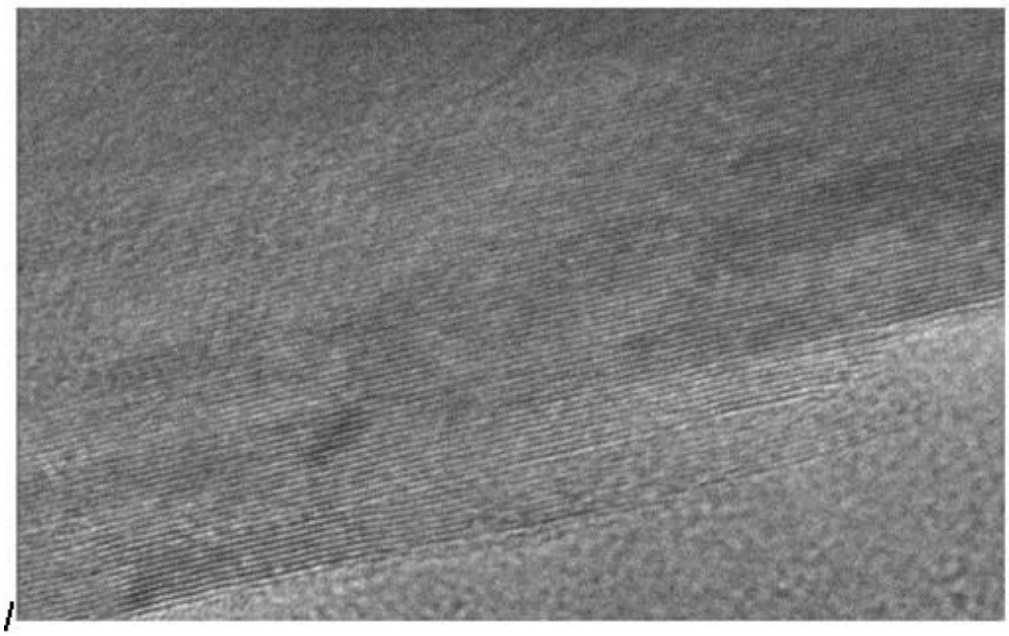

Figure 27 – 'High resolution' TEM images at nanometric scale showing the almost perfect stacks of large graphene layers, demonstrating that this SLA2 nuclear graphite is highly graphitised.

Image 28 (TEM, 11(0) dark field) confirms the presence of large crystallites exceeding 100 nm in size. This is consistent with XRD measured values (see Table 1). In addition, the presence of hkl reflections - particularly the good separation between 100 and 101 reflections and between 110 and 112 reflections - in the electron diffraction patterns (inset in Figure 28) points to the development of tri-periodic ordering in these large crystals making up nuclear graphite.

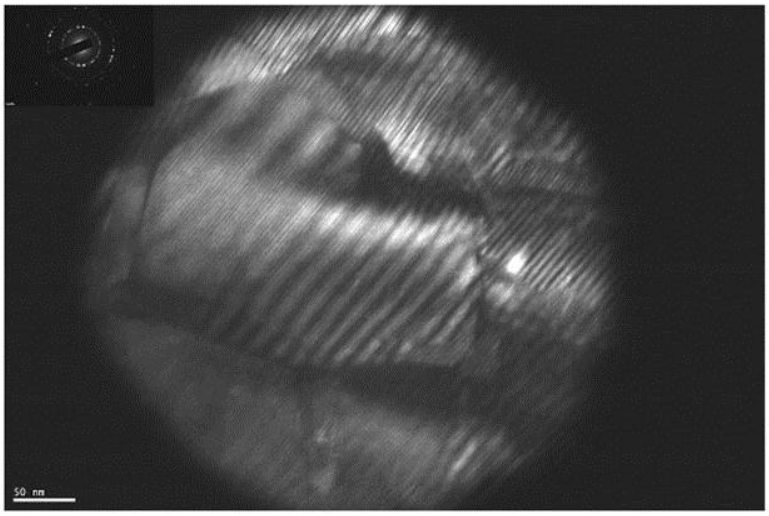

Figure 28 – TEM images in 11(0) dark field mode showing the size of SLA2 nuclear graphite crystallites (10 nm scale bar). Inset: SAED diagram showing punctual hkl reflections

4.2 Importance of graphite surface state in Raman spectrum interpretation

Figure 29 shows two scanning electron microscope images of the SLA2 graphite on two different scales. The density of this graphite is between 1.6 and 1.8 g/cm^3. The low apparent density with respect to monocrystalline graphite (density = 2.265 g/cm^3) can be explained by the fact that nuclear graphite is very porous (with pores and cracks at the boundaries between the petroleum coke and coal-tar pitch coke and within the latter).

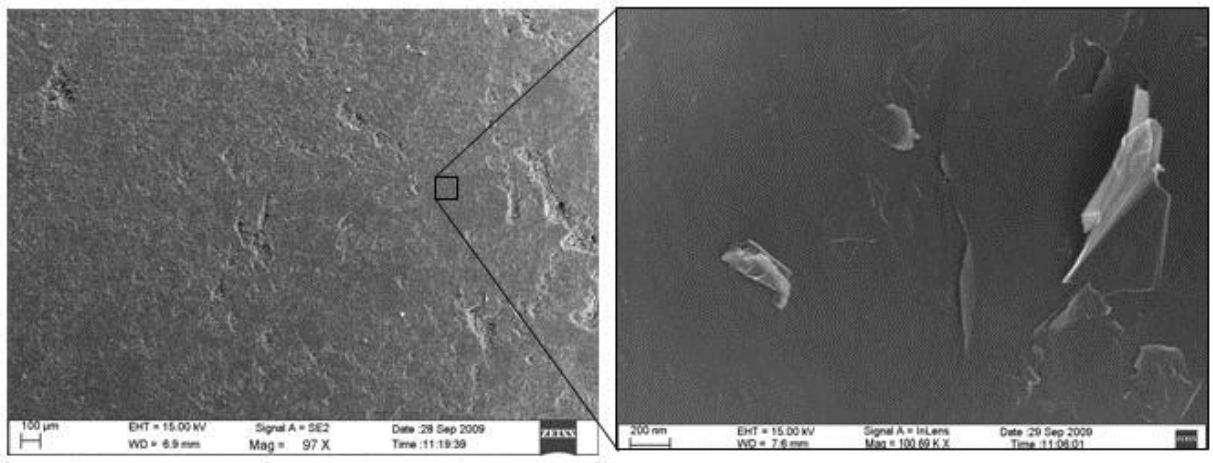

Figure 29 – Saint-Laurent-des-Eaux (SLA2) virgin graphite seen under the scanning electron microscope; the low-magnification image on the right shows the pores between grains of petroleum coke; the image on the left, with higher magnification, shows the lamellar texture of a highly graphitised petroleum coke grain

When using optical polarising microscopy *to distinguish the various components making up nuclear graphite* (which, as we have already seen, is really a highly graphitised carbon-carbon composite) or when preparing this material for SIMS analysis, *it is essential for material surfaces to be perfectly plane and polished. One of the main problems with polishing, however, is the sensitivity of the defect band intensity to the surface state of the sample under analysis. This sensitivity has often been recognised.* The consequence of this is the notable growth of the D_1 and D_2 bands (see Figure 30 on the next page).

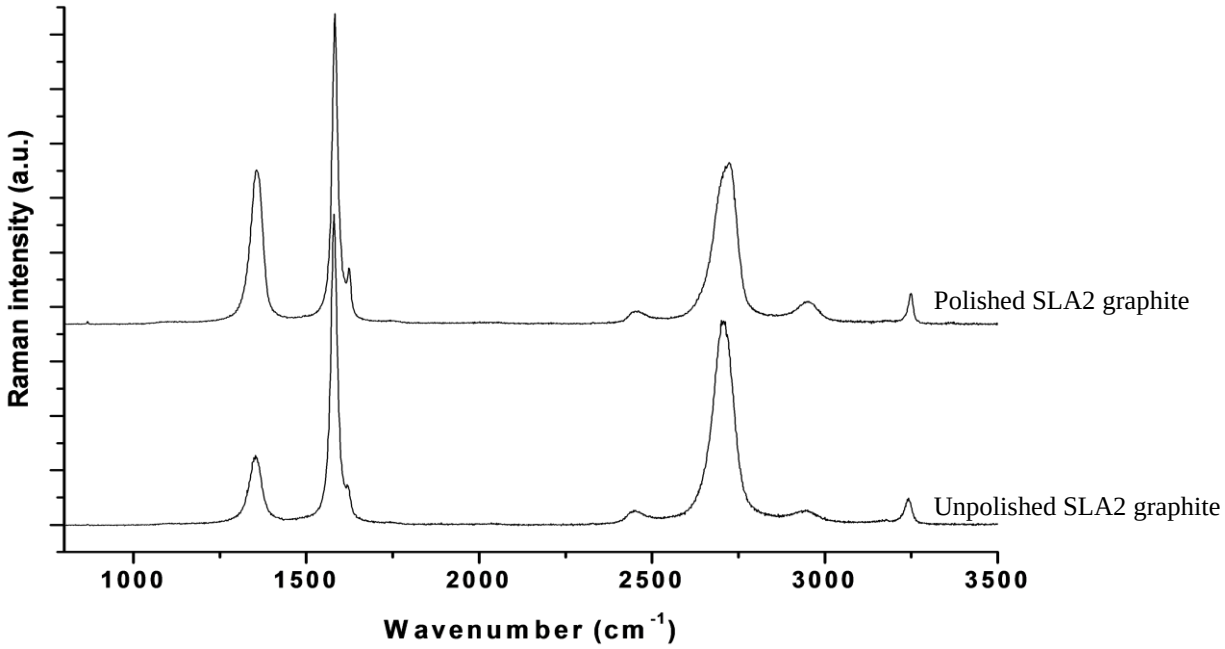

Figure 30 – Raman spectra of polished and unpolished SLA2 nuclear graphite, illustrating the very significant growth in the D1/G intensity ratio due to polishing

This increase in the D_1 band induces unacceptable errors in the structural characterisation of these polished graphites. Polishing has a major impact on determining the degree of intrinsic disorder and is responsible for errors in determining the average size of crystallites, L_a, often calculated by I_{D1}/I_G ratio measurements and applying a 'Tuinstra et Koenig' formula (see page 13).

Specialists in carbon Raman spectrometry have already recognised the effect of surface preparation and a few 'tricks' have been suggested for eliminating these polishing artefacts. Geologists, for example, propose using the confocal system of the Raman spectrometer to focus the laser excitation light on a carbon surface that is entirely protected by overlying transparent mineral phases. This process cannot be used, however, for the study of nuclear graphites which only consist of completely opaque phases (cokes).

To learn more about this phenomenon and guarantee completely reliable structural characterisation of our samples, we studied the effect of polishing on anthracene cokes

characterised by varying degrees of disorder (materials undergoing pyrolysis at temperatures of 1600, 2000 and 2900°C). For this purpose, millimetric grains were coated in an epoxy resin, then polished with diamond pastes containing different sized diamond particles (6.3 and 1 µm) to obtain various surface states.

Figure 31 shows the full width at half maximum of the G band as a function of the D1 and G band intensity ratio. As demonstrated earlier, linear behaviour between these two parameters is observed in the graphitisation domain (red line).

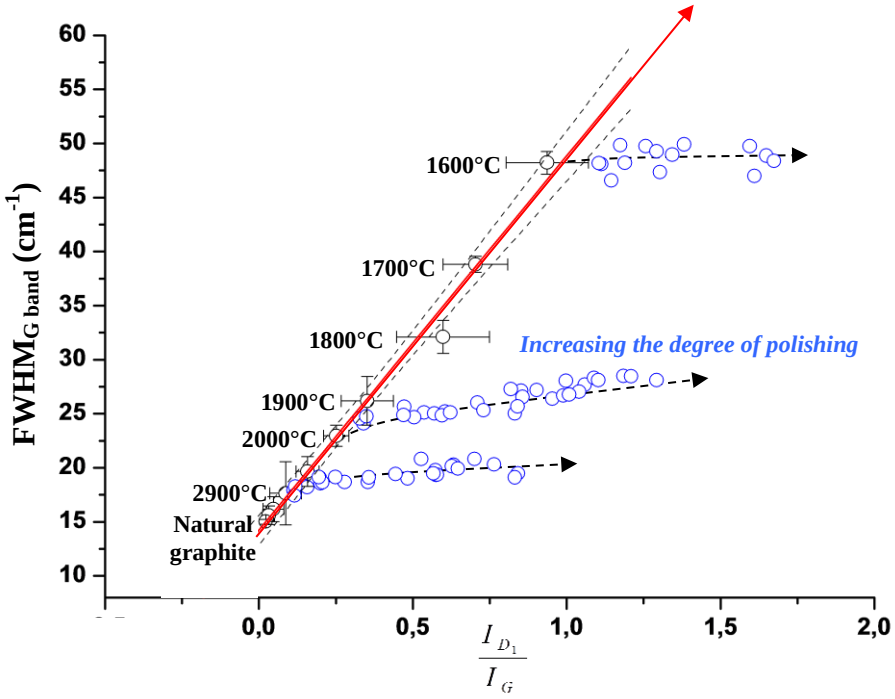

Figure 31 – Changes in the FWHM as a function of the D1 and G band intensity ratio in polished (blue dots) and unpolished graphitisable carbons (black dots)

Contrary to the assumptions made by several authors concerning polishing-induced damage in carbonaceous materials, it is clear that this process is responsible for very little structural disorder in the strict sense of the term. This can be seen in the fact that the FWHM of the G band in anthracene coke obtained at 2900°C, only varies by 16.2 ± 1.2 to reach 20.3, although the intensity ratio increases by 0.04 ± 0.03 to 0.76). This type of degradation due to

this polishing is obviously far 'milder' than the major structural changes (which XRD and HRTEM measurements have shown can reach almost complete amorphisation) induced, for example, by highly energetic mechanical grinding of the graphite for several hours **[7]**.

We therefore very strongly recommend using the FWHM of the G vibrational band as a reliable parameter, at least in the case of polished carbonaceous materials, to determine the degree of intrinsic disorder and, more especially, their degree of graphitisation.

These recommendations were put forward at the last annual meeting of the GFEC, which was held in Gréoux-les-Bains from 29 March to 1 April 2010, and at the Carbon 2010 World Conference held at Clemson University in South Carolina, USA, from 11 to 16 July 2010. A paper is now accepted by Journal of Raman Spectroscopy.

5 Simulation of neutron irradiation by ion implantation

Experiments to implant chlorine-37 ions in graphite structural consequences

N.B. Given the absence of samples from European nuclear plants expected for the Carbowaste programme and the very late delivery to CEA Saclay of samples of used nuclear graphite from french nuclear power plants (Saint Laurent des Eaux et Marcoule), we carried out a structural study of the effects of irradiation using analogues made up of graphites with non-radioactive ions implanted in them. Using non-radioactive objects, we were then able to study samples representative of fluences, temperatures and impurities comparable to those to which graphites are subject inside nuclear reactors during operation.

The experiments and characterisations using neutron-irradiated graphite are not so simple to perform, since they require a number of conditions and precautions due to the radioactivity; this is therefore very expensive and very time-consuming compared to examining non-radioactive analogues. However, the structural changes in materials due to irradiation can also easily be obtained using all sorts of energetic particles: electrons, protons and ions, thereby producing defects that are relatively simple to characterise using non-radioactive graphites.

Among the particles mentioned above, ions have the advantage of producing very quickly, in just a few hours or even a few minutes in the case of certain fluences, a large number of displacements of atoms, comparable to those obtained inside a nuclear reactor after a year of neutron irradiation. In addition, since they are typically produced within the energy range from one to several hundreds keV, they are mainly slowed down by elastic collisions. Above all, 'nuclear braking' causes the displacement of atoms in cascades, known as 'dense collision cascades' (see figure below), which is probably similar to the displacements produced by neutrons.

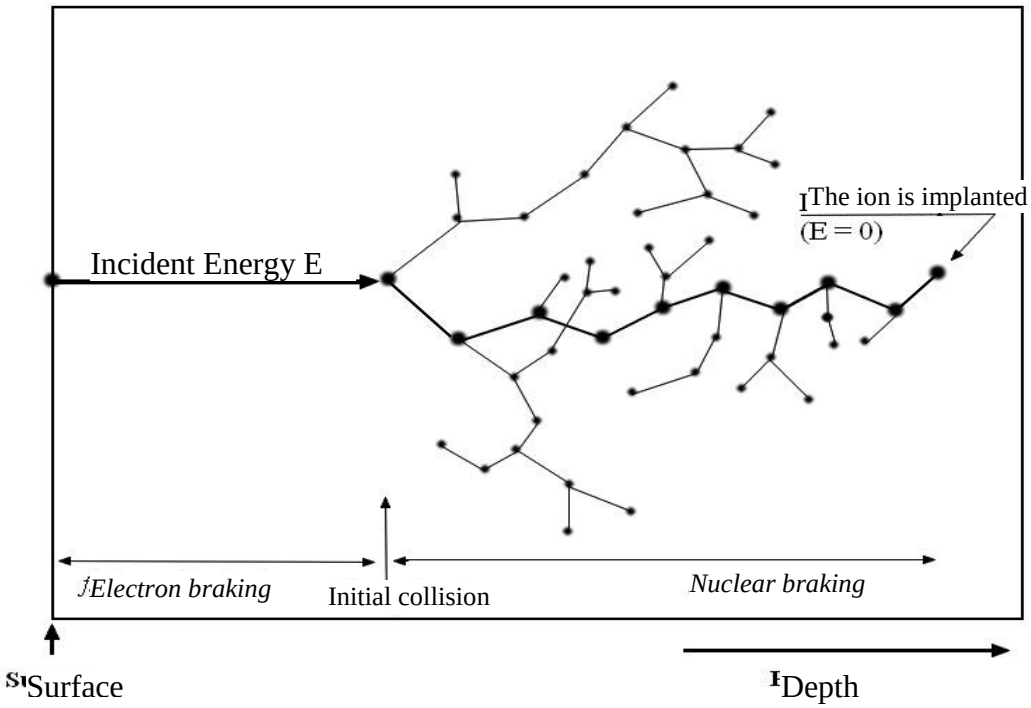

Path of a particle implanted in matter with an incident energy E

For this study, ^{37}Cl ions were used in an attempt to simulate the effects of neutron irradiation in nuclear graphite, and, in particular, to identify the key parameters that influence structural changes in nuclear graphites inside a reactor. The major challenge, however, will be to check the equivalence of the results obtained for neutrons irradiation and for ions implantation.

Ion implantation was carried out using the 400-kV ion implanter at the Institute of Nuclear Physics of Lyon (IPNL), as part of a collaboration project with Nathalie Moncoffre, Nelly Toulhouat and Claire-Emilie Vaudey.

The instrument is conventionally made up of three pieces of equipment: the ion source, the mass analysis electromagnet and the Faraday cup collector, as shown in Figure 32.

- The **ion source** consists of a graphite chamber and a hot tungsten cathode which emits electrons that ionise the injected gas into which the chemical compound is usually vaporised in the form of a chloride. In the case of highly refractory elements, compounds are doped with chloride *in-situ* by injecting carbon tetrachloride in the furnace, which can be heated to a temperature of 1,400°C. The ions created are then accelerated due to the potential difference between the source (at the high voltage of 30 kV) and the accelerating electrode (at a voltage of -400 V).

- The mass analysis **electromagnet** then separates out the ions according to the ratio q-to-m, where q is the charge of the ion and *m* is the mass of the ion.

In the **Faraday cup collector**, a diaphragm limits the beam of ions to be implanted in the target, which is at ground potential. A grid, to which a voltage of -500 V is applied, is used to recapture electrons ejected during implantation on the target-holder to obtain an accurate measurement of the number of charges received by the target. Integration of this current indicates the dose of implanted elements and homogeneity is ensured by scanning the beam with an electrostatic X/Y scanner.

The ion implanter works with a vacuum of 10^{-4} Pa in the implant chamber, obtained thanks to a combination of turbo molecular and cryogenic pumps. *The samples were implanted with ^{37}Cl with an energy of 250 keV and at various implantation fluences (from 10^{12} to 10^{16} ions/cm^2) and temperatures (25°C to 600°C).*

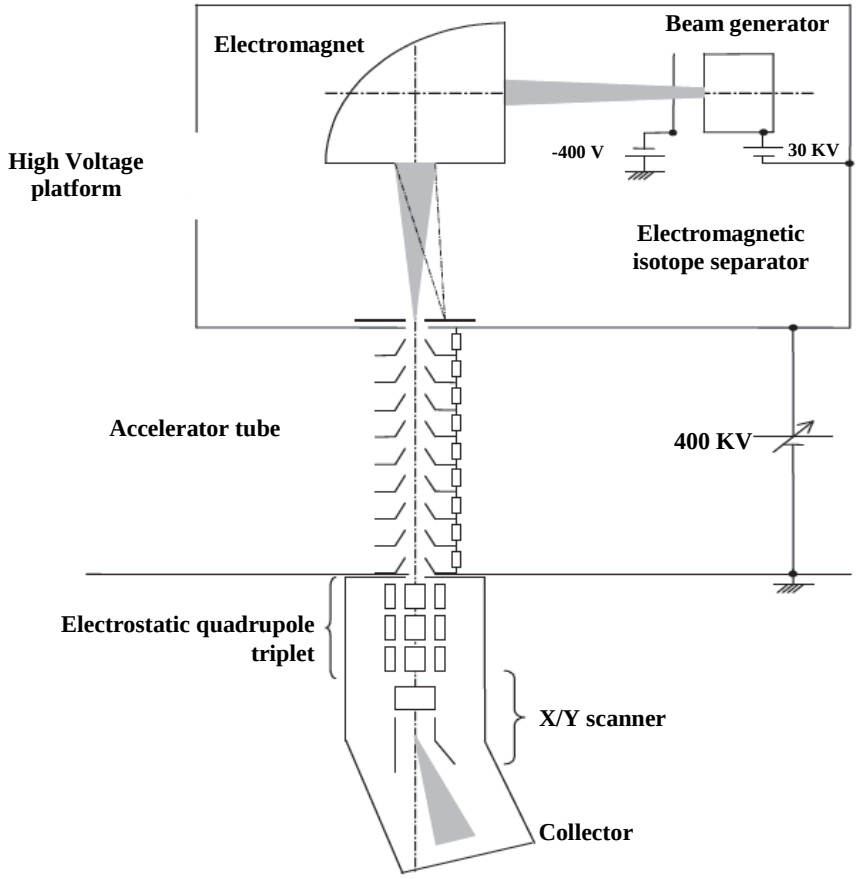

Figure 32 – Diagram of the IPNL's high energy implanter-separator.

5.1 Effect of fluence

It is important to point out that the interactions and displacements caused by charged chlorine particles are not the same as those created by neutrons due to the electron and nuclear energy lost upon collision. Figure 33 shows the dominance of the energy loss mechanism in the case of ion-solid interaction. It shows the electron and nuclear stopping power in relation to the energy of the implanted particle.

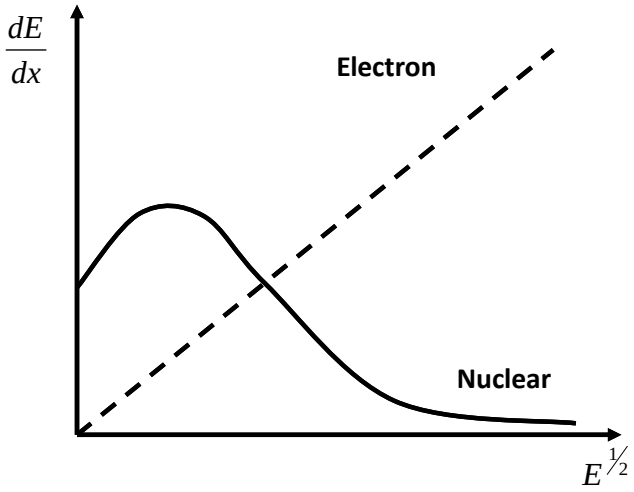

Figure 33 – Stopping power in relation to ion energy in the case of ion-solid interaction

Obviously, a low energy should be chosen, so that nuclear collisions will dominate, thereby producing dense cascades. On the other hand, in the case of Raman characterisations, where laser beam penetration in the graphite is only around 100 nm, a compromise with regard to energy must be made in order to analyse the entire area destructured by implantation whereas the dominance of nuclear interaction is conserved.

To highlight the effect of fluence on the structure of nuclear graphite, the samples were implanted with ^{37}Cl at different fluences ranging from 10^{12} to 10^{16} at.cm^{-2}.

Table 2 shows the quantity of defects created at implantation depth Rp depending on implantation fluence, together with the total number of defects created within the implanted area, calculated using the whole defect profile.

Implantation fluence (in ions/cm²)	Quantity of defects created at maximum concentration in the defect profile (in dpa)	Total quantity of defects created (in dpa)
10^{16}	7.1	88
10^{15}	0.5	8.8
5.10^{14}	0.2	4.5
10^{14}	0.05	0.9
5.10^{13}	0.02	0.4
2.10^{13}	0.008	0.16
10^{13}	0.004	0.08
10^{12}	0.0004	0.008

Table 2 - Defects created by implanting 37Cl in nuclear graphite (SLA2), with an energy of 250 keV.

Figure 34 (next page) shows the different Raman spectra, within the spectral range 800 - 3500 cm^{-1}, of nuclear graphite (SLA2) implanted at different fluences, at ambient temperature and with energy at 250 keV. These spectra are compared with that of a standard monocrystalline graphite, HOPG, and a *reference amorphous carbon* obtained by condensing a carbon vapour at ambient temperature and in a vacuum of 10^{-6} torrs. For clarity, the spectra were normalised relatively to the G band.

These spectra clearly show significant variations in the different bands as fluence increases, in the first- and second-order spectra. At a first stage, these variations are related to an increase in relative intensity of the D_1 band and a decrease and significant widening of the G band as well as all of the second-order bands. During this first regime, the significant increase in the ratio D1/G represents an increase in disordering.

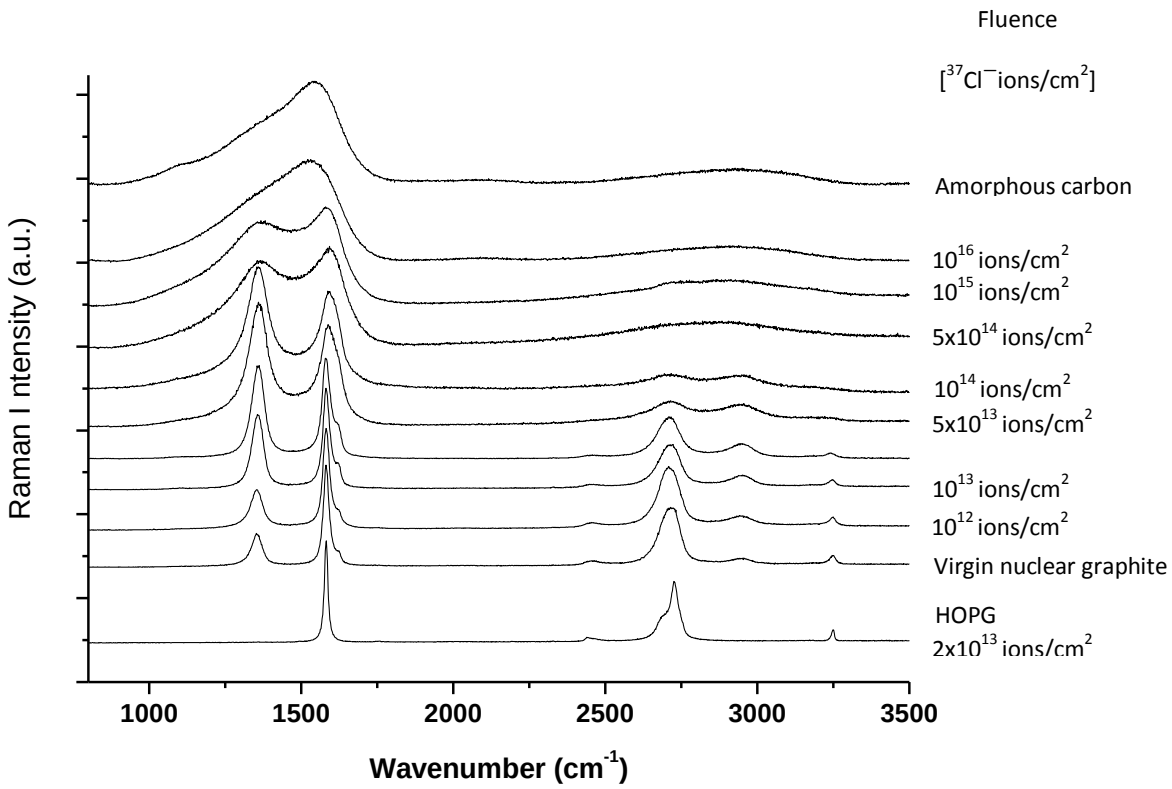

Figure 34 – Variations in the first- and second-order Raman spectra of 37Cl+-implanted graphite at different fluences and at ambient temperature

Above $5x10^{14}$ ions/cm^2, it seems that a second regime of structural degradation is achieved: in fact, G and D_1 bands broaden and become faint. Ion implantation has caused significant damage to the crystalline structure of the nuclear graphite. *At higher fluence (above 10^{16} ions/cm^2), the crystalline structure has completely disappeared, and the nuclear graphite thus tends to become amorphous in the strict sense of the word*, resulting in the presence of a single very large asymmetric band at a maximum of 1540 cm^{-1}; the Raman spectrum of the graphite implanted at this fluence is similar to that observed for the totally amorphous carbon used as a reference. It can therefore be expected that the resulting carbon will be formed only of very small and badly stacked polyaromatic structures, or even that it would contain sp3 carbons.

To monitor the changes in structural defects caused by ion implantation of graphite at depth, we used a sample of nuclear graphite implanted at a fluence of $5x10^{13}$ ions/cm^2, in which the defects band D1 appears clearly, and we cut it in two. We then analysed the section

edge using Raman microspectrometry. The analysis was performed automatically with a step of 0.5 µm, thanks to the microspectrometer's motorised stage. Each acquisition lasts 60 seconds. Figure 35 shows the variation in R_2 surface ratio (= D1/D1+D2+G) depending on the point along the line analysed. The plotting is used to verify the transition from an ordered graphite structure to a disordered carbon structure along the side implanted.

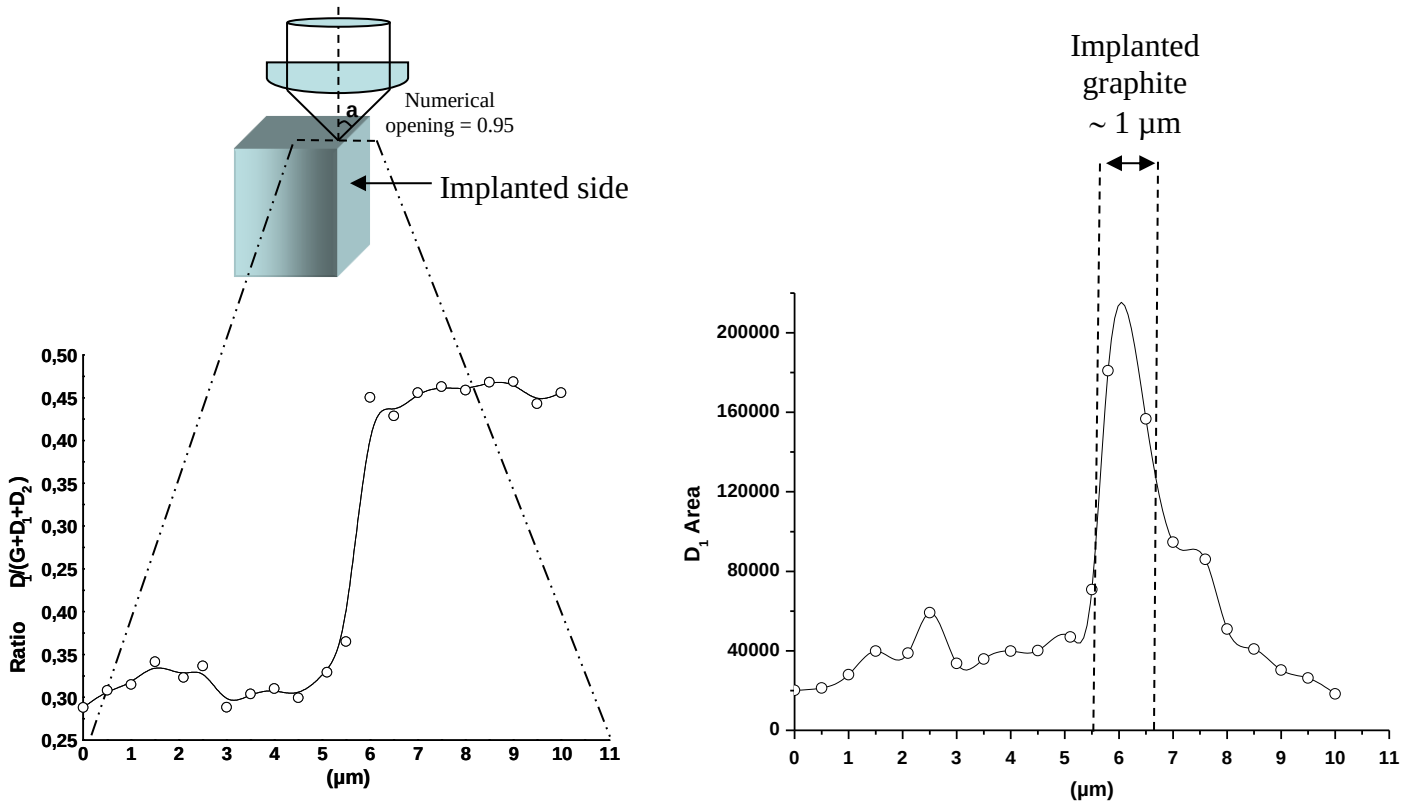

Figure 35 – Change in the integrated intensity of D1 relative to all the bands, i.e. R2 ratio, depending on the depth analysed and showing (a) the transition from an ordered to a disordered structure of the graphite, and (b) the thickness of the disordered area caused by ion implantation.

The thickness of the disordered area was measured using the same technique, this time to observe the integrated intensity of the D1 band.. The thickness of the disordered area (~1 µm) was estimated based on the full width at half maximum of the Gaussian band. It well agrees with the theoretical value.

The result, obtained using micro-Raman spectrometry, shows the chlorine's shallow penetration, thereby causing defects at the subsurface (~ 1µm).

Nonetheless, *due to such thinness, it is not possible to directly or easily visualise the damage caused, at the nanometric scale, using conventional object thinning techniques required for TEM. To do this, we used a recently-developed technique for cutting thin infra-micrometric sections of a solid object, using a Focused Ion Beam technique (FIB).*

The equipment used is a 'Dual Beam' equipped with two guns (Figure 36): an electron gun and a gallium ion gun. The electron source is used to image the surface of the sample according to the same principle as a conventional scanning electron microscope (SEM). The second gun emits a beam of Ga ions, the voltage (5-30 kV) and the intensity (1-20 µA) of which can be adjusted.

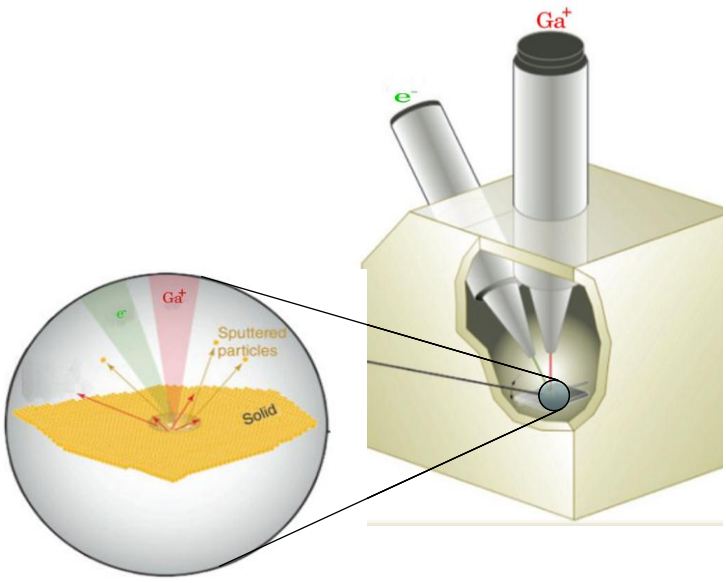

Figure 36 – How the FIB technique works

By positioning the ion beam precisely, it is possible to erode the object into any shape desired. It is this ion beam that is used to cut ultra-thin sections (< 100 nm, i.e. transparent to electrons), with a surface area of 15 µm×5 µm from the samples of nuclear graphite. These can then be observed using TEM (see Figure 37, next page).

Our FIB sections were cut using an FEI STRATA DB 235 Dual Beam system at the IEMN (the Institute for Electronics, Microelectronics and Nanotechnology in Lille, France), assisted by David Troadec.

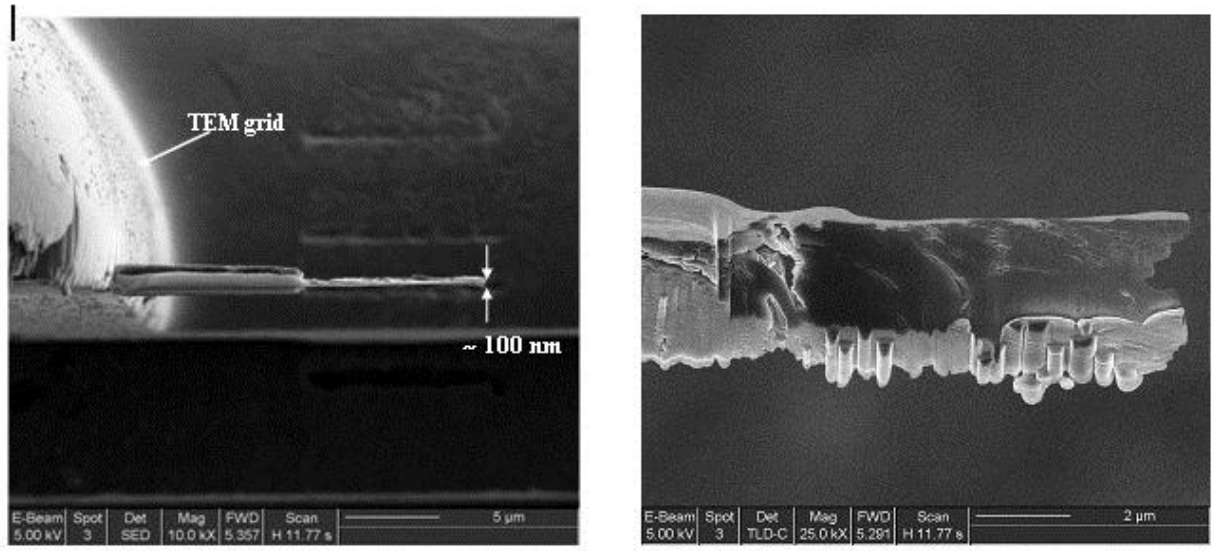

Figure 37 – Scanning electron microscope images obtained for an ultra-thin section of nuclear graphite achieved using FIB method

In the studies carried out using thin sections prepared using FIB (see Figure 38a, next page), the surface of the implanted graphite appears at the top of the section, just below the protection layer (see arrow on image 38b). These sections are thin enough to perform a TEM imaging in High Resolution mode and thus visualise the graphene plane profile. Thus, at nanometric scale, we can observe from the surface where the graphite suffered the greatest damage due to implantation (Figure 38c) down to the virgin graphite (Figure 38e) which was not implanted, just a few micrometres below the surface, passing through an area less damaged by ion implantation (Figure 38d).

These images confirm the structural changes revealed by Raman microspectrometry and allow us to directly visualise the effects of implantation on the structure of the graphite.

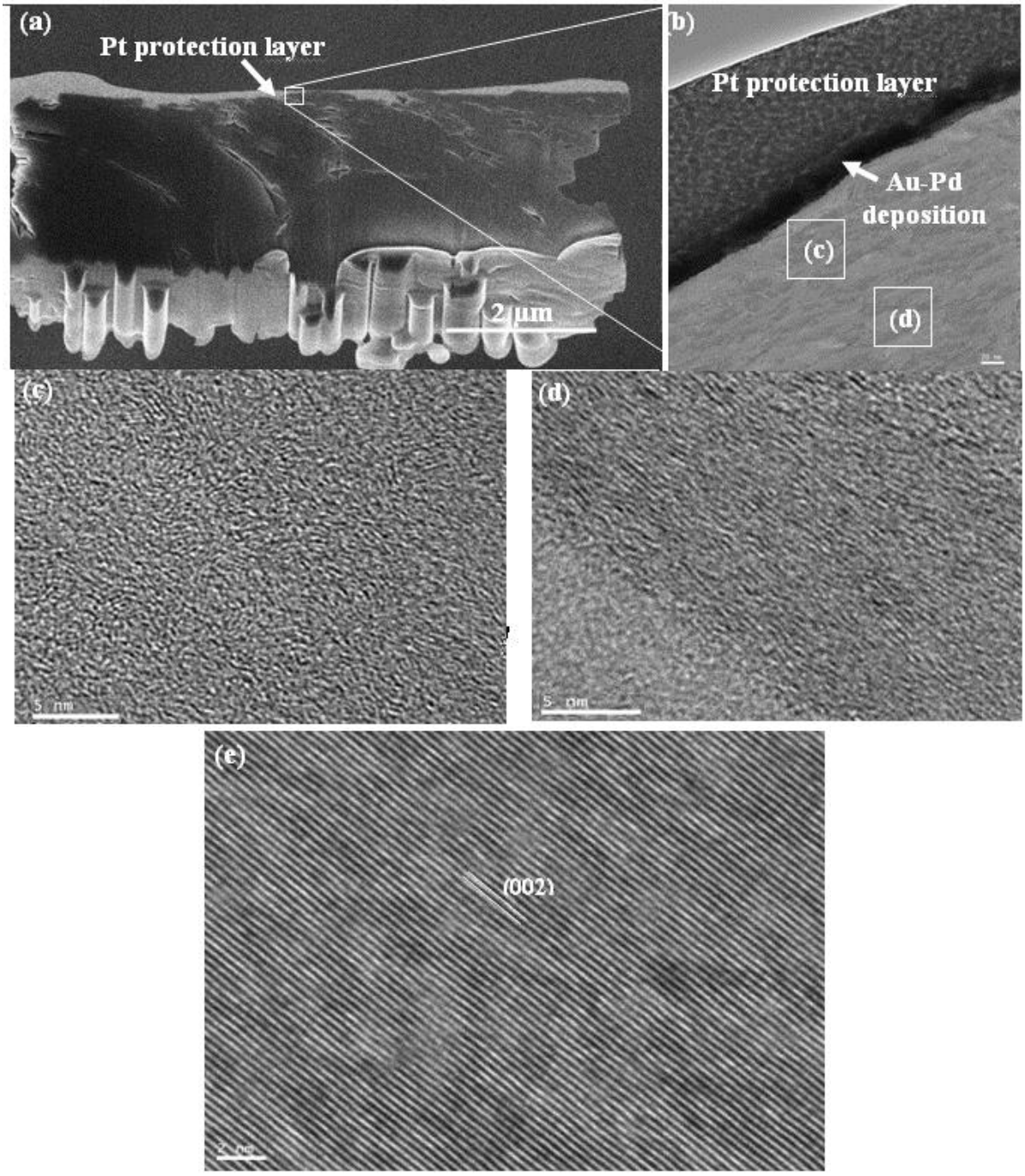

Figure 38 – (a) SEM image ('secondary electron' mode) of a thin section, prepared using FIB, of graphite implanted at fluence of 5x1013 ions/cm2; (b) TEM image of the implanted graphite. c), d), e) HRTEM images (in 002 lattice fringe mode) showing the structural degradation of the graphite following 37Cl implantation, increasing from the outer surface (the most highly implanted) to the core (virgin graphite).

The HRTEM images show an extremely substantial change in how the polyaromatic layers are organised in areas close to the surface, i.e. where the implanted chlorine is at its maximum density. Image 38c shows that the layers extent here are very small (around a nanometre) and the stacks are composed of only a few layers. In addition, these stacks are randomly oriented. *In geometric terms, such disorientation of the stacks creates nanometric-sized holes, forming nanopores. These are potential sites for trapping elements located or ejected outside the aromatic cycles, ^{37}Cl as in this case, or ^{36}Cl and ^{14}C in the irradiated nuclear graphites.* As we move deeper below the surface, the concentration of implantation becomes lower, and the graphene layers are less distorted and better stacked, as shown in image 38d. At a depth of a few micrometres, there is no implantation at all and we see the original virgin graphite formed of perfectly-stacked large graphene layers (image 38e).

While high resolution imaging provides information on the height of stacks forming coherent domains (L_c), images in 11 dark field mode provide complementary information as the L_a diameters of coherent domains, somewhat incorrectly called 'crystallites', by measuring the extent of the homogeneous moiré fringes (i.e. with the same period and same orientation). These 11(0) dark field images confirm that the La decrease as we move nearer the surface and, therefore, for increasing concentrations of implantation. The size of the largest coherent domain is 200-300 nm in the case of virgin graphite, and 50-100 nm in the implanted area with the highest implanted ion concentration (Figure 39) ; the crystallites are then replaced by small nanometric coherent domains characterised by a few moiré fringes.

The TEM results thus entirely agree with the Raman results (width of G band, I_D/I_G ratios). The success of this combination of TEM and Raman imaging using FIB sections of implanted graphite is a world first. A paper on the subject was published in Carbon in 2010.

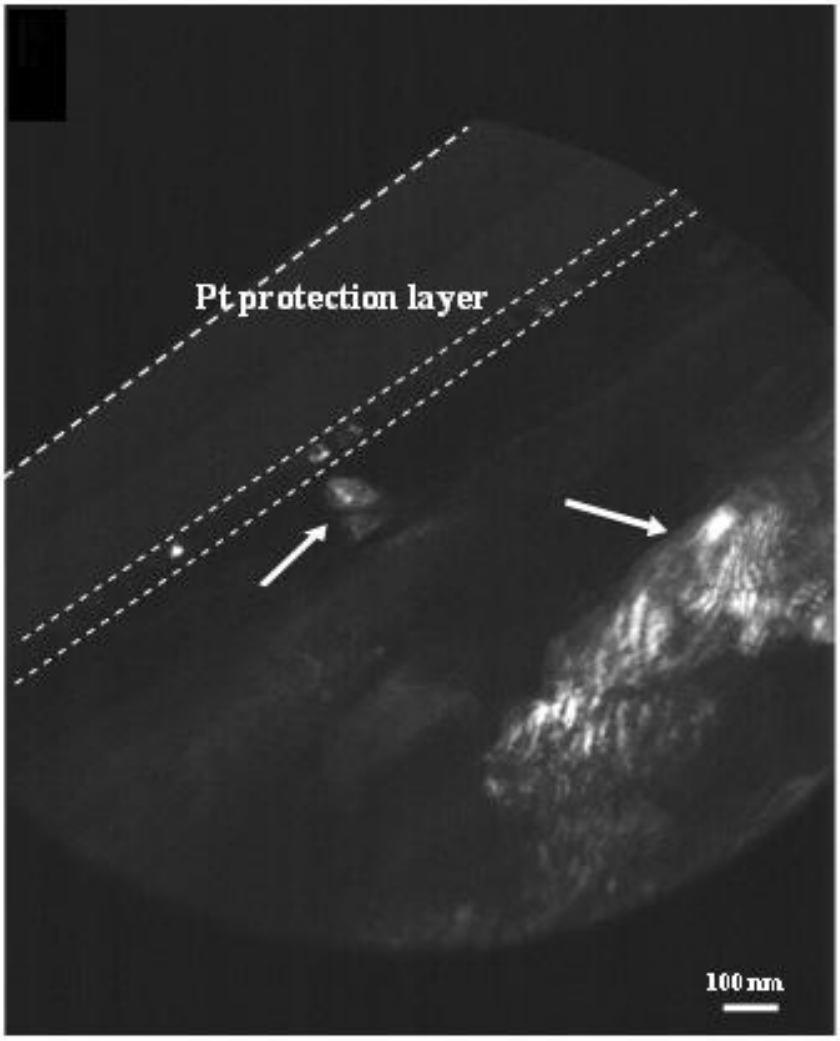

Figure 39 – 11 dark field image of an FIB section of implanted graphite showing significant decrease in the size of crystallites near the surface, where there is maximum implantation.

5.2 Effect of implantation temperature

In the case of graphites subject to neutron irradiation, it is well known that irradiation temperature is a key parameter for understanding the mechanical and thermal degradations of graphite in a nuclear reactor. *Using analogues, we assessed the effect of implantation temperature on the nanostructure of nuclear graphite. Our Raman microspectrometry studies confirmed that implantation temperature does have a major effect on structure.*

Figures 40a and b are the Raman spectra within the frequency range 800-3500 cm^{-1} of nuclear graphite implanted at fluence of $5x10^{13}$ at/cm^2 and 10^{16} at/cm^2 respectively, for various temperatures of implantation from the room temperature to 600°C. Figure 40a shows that there is an effect marked by a progressive and significant decrease in the D_1 defect band as the implantation temperature rises, until reaching a structure similar to that of virgin graphite (low intensity D_1 defect band). *This indicates a competition between irradiation, on the one hand, which tends to destructure the material and, on the other hand, the temperature, which tends to repair the damage, thus promoting the recombination of defects as soon as they are generated*. At much higher fluence (i.e. 10^{16} at/cm^2, Figure 40b), the implantation temperature range used is no longer high enough to promote such repair and the graphite is structurally degraded, although it is not totally amorphised.

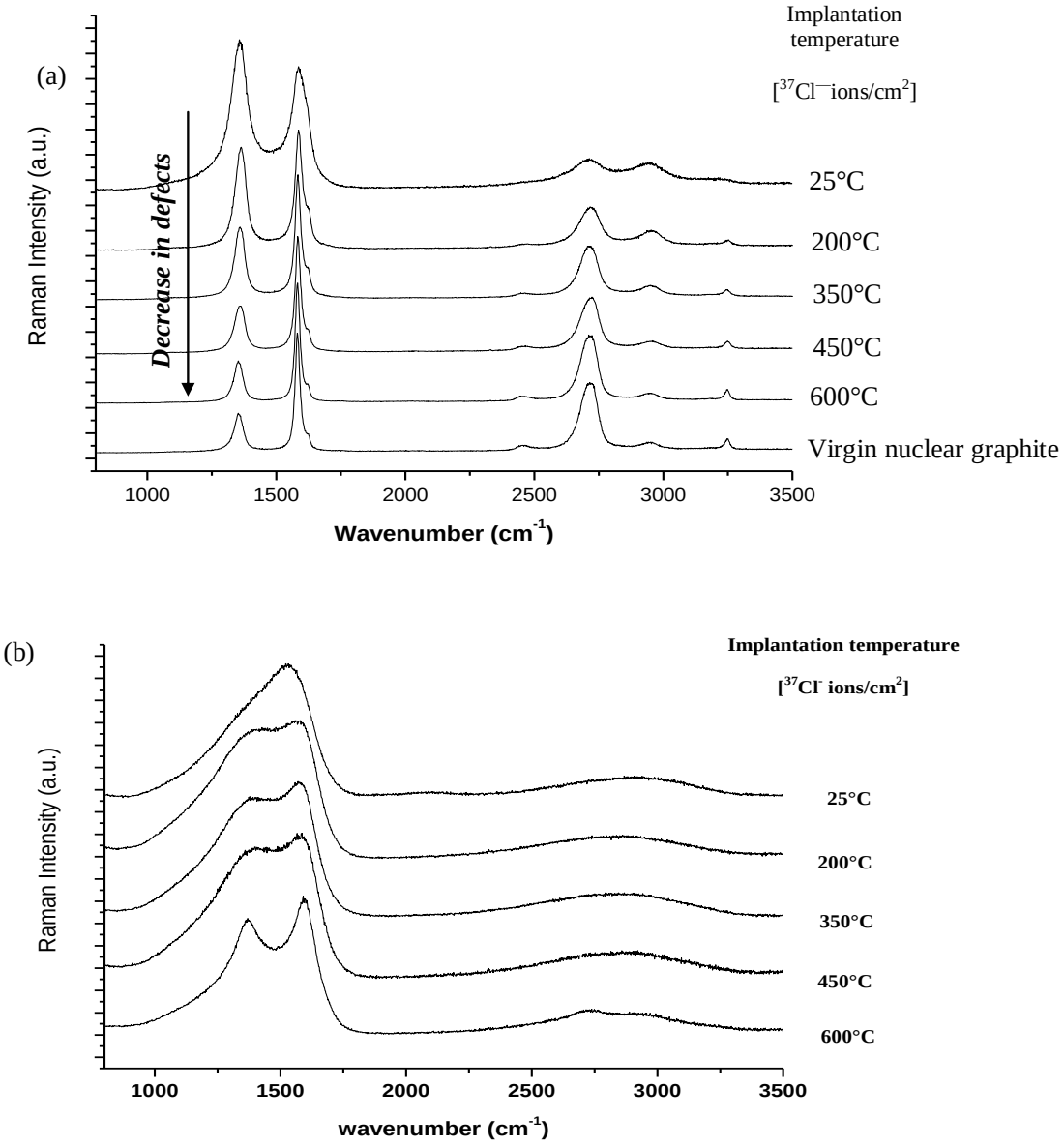

Figure 40 – Raman spectra of nuclear graphite implanted with chlorine-37 at various implantation temperatures and fluence of: a) 5x10^{13} ions/cm^2 and b) 10^{16} ions/cm^2.

Figure 41 shows the structural change in the graphite under the double effect of heat treatment and ion implantation. It is clear that structural degradation due to implantation follows a path in the diagram below where the 'width of the G band (FWHMG) according to the ID1/IG ratio (R_1 ratio)' which is completely different to the path followed during graphitisation. This means that the effect of implantation cannot be thought of as an exact

inverse of the effect of graphitisation. It should be noted that, in this diagram, we see two different ion irradiation regimes: one is linear at low fluence and the other at high fluence. In addition, it is highly probable that this rapid increase of the defect band is also due, among other things, to the ionisation of carbon atoms during ion irradiation and not only to the decreasing size of coherent domains.

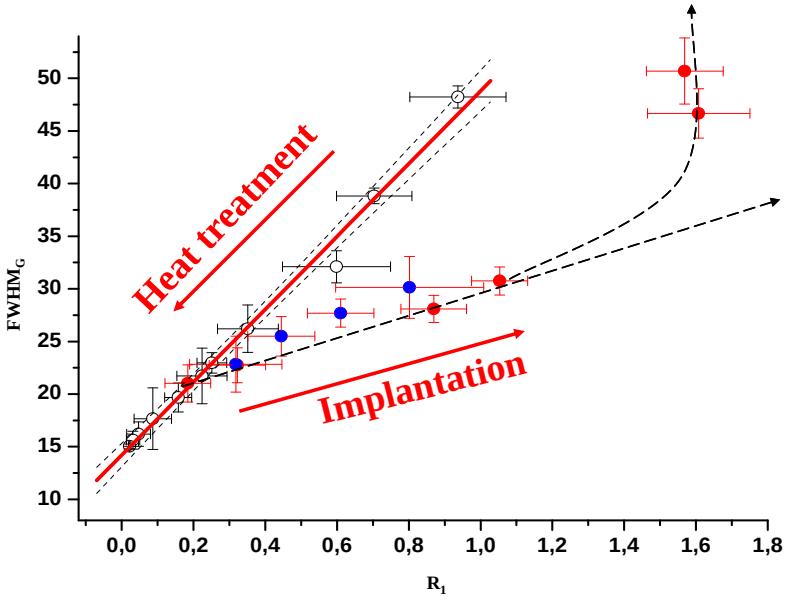

Figure 41 – Change in full width at half maximum of the G band in relation to the intensity during thermal graphitisation and ion irradiation.

From a practical point of view, these results challenge the 'universality' of the calibration proposed by Tuinstra & Koening, which should only be used for carbons subject to 'normal' graphitisation; other laws are needed for estimating crystallite size in the case of ion-irradiated carbonaceous materials.

6 Characterisation of two irradiated nuclear graphites (G2, SLA2)

Within the framework of this contract, all the characterisations of these radioactive samples (by X-ray diffraction, Raman microspectrometry and TEM) were performed at the CEA/Saclay *Laboratoire de caractérisations Physico-Chimiques des matériaux Irradiés* (Laboratory for the physical and chemical characterisation of irradiated materials) which is

certified for working with radioactive materials, in collaboration with Lionel Gosmain and Bénédicte Verhaeghe. In 2010, we examined two irradiated graphites from the nuclear power plants located at Marcoule (G2) and Saint-Laurent-des-Eaux (SLA2).

G2 nuclear graphite

The G2 reactor (Figure 42) was built in 1958 and is one of three prototypes (G1, G2 and G3) in the GCR [gas-cooled (graphite-moderated) reactor] series, designed to produce military-grade plutonium. It was shut down in 1980 and is currently being dismantled.

Figure 42 – Marcoule G2 and G3 nuclear reactors

Figure 43 is a sketch of the G2 reactor. It is characterised by its horizontal position and consists of a stack (the moderator) and a reflector, both of which are made of graphite. The stack is an array of columns made of graphite bricks with an hexagonal section and arranged so as to form channels to allow fuel elements to be introduced. The reflector is located at the periphery of this reactor. It is made of the same type of bricks, but of higher density (2 stages of impregnation instead of one during composite production). In addition, underneath the stack there is a support area, also made of graphite, which provides biological protection.

The G2 graphite samples studied come from the 9.4m-high vertical radial core sample taken in September 1989. Since the coolant gas (CO_2) circulated laterally, the irradiation

temperature was practically the same for all the samples (approximately 300°C). However, it is possible that the graphite located close to the reactor core was slightly hotter (by around 10°C) than the areas further from the core. Samples 27 and 32 of the moderator were located close to the reactor core. Sample G2-42 of the moderator, however, was far from the core, while sample 46 is the only sample taken from the reflector.

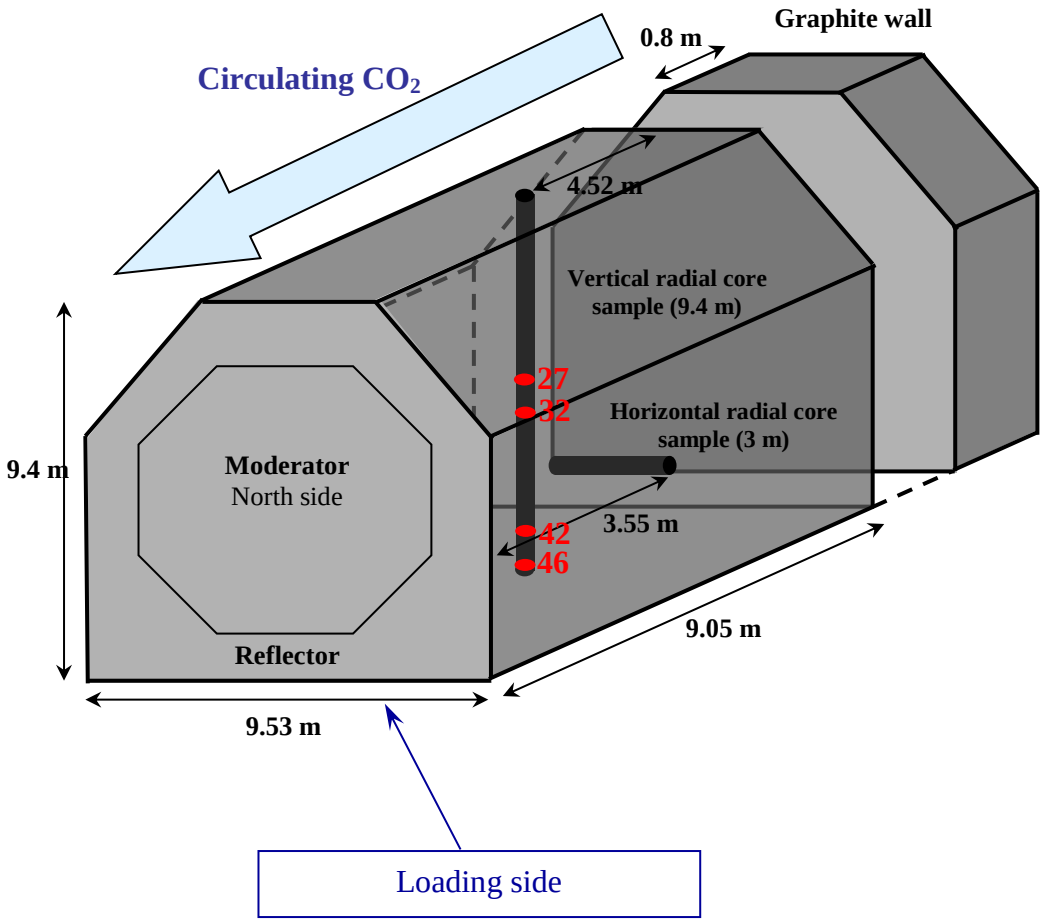

Figure 43 – Sketch of the 'horizontal' G2 reactor, consisting of a graphite stack (moderator) and a reflector (made of high-density graphite), and showing the location of the samples examined in this work.

The G2 and SLA2 nuclear graphites were first characterised using methods of 'global' analysis : X-ray diffraction (XRD) provides data on the volume of the samples to the cubic millimetre scale and Raman microspectrometry to the cubic micrometre scale.

Figure 44 below shows the 002 reflection profiles (left) and the 10.0 and 10.1 reflections (right) for four G2 irradiated graphites. Compared with the fine 002 line, centred at d_{002} = 0.3365 nm for the virgin graphite[1], the 002 lines for the irradiated graphites are somewhat broader and their maximum tends toward small angles (corresponding d_{002}: 0.3400 nm). This means that the average height of the crystallites (L_c) decreases and the spacing between layers increases.

With regard to hkl reflections (diffractogram on the right), 10.1 reflection intensity is much stronger than that of the 10.0 for the G2 virgin graphite (in blue), confirming a high level of graphitisation. On the other hand, the intensities of these reflections become similar for the irradiated graphites, confirming degradation of the tri-periodic ordering.

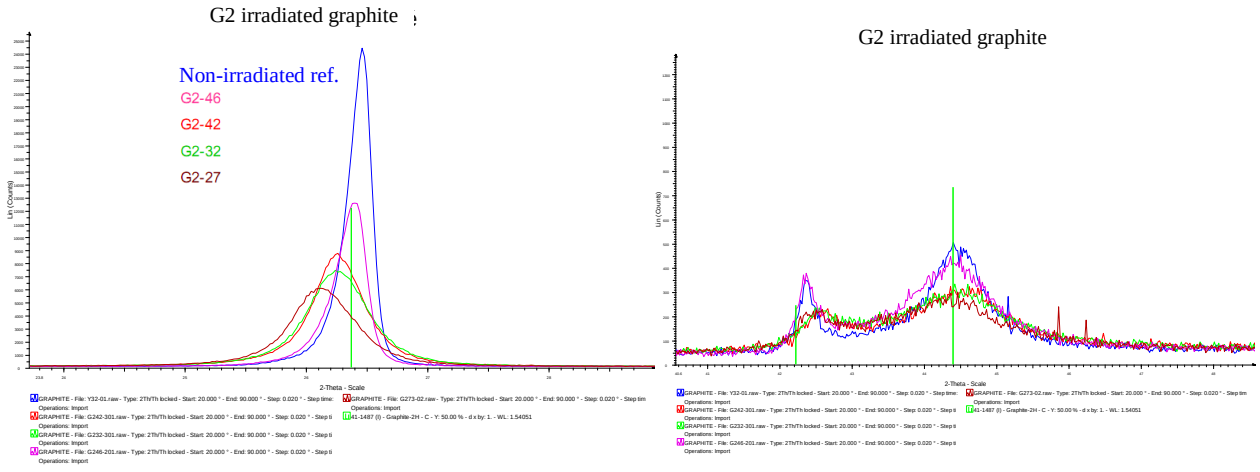

Figure 44 – Diffractograms of G2 nuclear graphites – virgin and irradiated; left: 002 reflection profile, right: 10.0 and 10.1 reflection profiles.

[1] theoretical value of 'true' graphite: d_{002} = 0.3354 nm

To characterise the structure of the G2 irradiated graphite, structural characterisations were performed using a Raman microspectrometer at the CEA with a specially adapted unit linked to the laser by an optical fibre (‘hot stage analysis’, see photos below). The experiment conditions (exciter wavelength, polarisation etc.) were identical to those used to examine the virgin graphite with the Renishaw microspectrometer at the ENS in order to have a reliable comparison of the results obtained using the two microspectrometers.

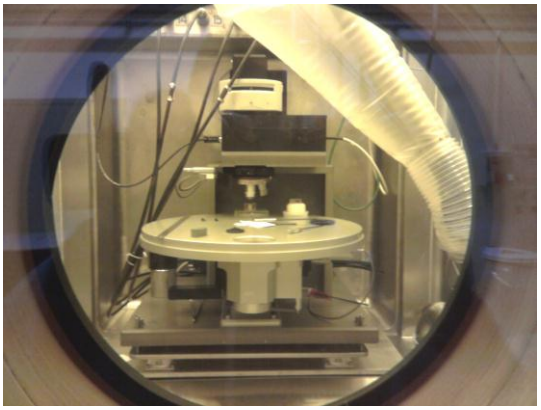

Figure 45 – Raman microspectrometry equipment at the ‘Laboratoire de caractérisations Physico-Chimiques des matériaux Irradiés’ designed for studying radioactive materials

Figure 46 shows two Raman spectra of the G2 virgin and irradiated graphite (G2-27). A structural change in the graphite due to neutron irradiation is clearly apparent. As for ion irradiation (implantation), this is characterised by a significant increase on the intensity of the D_1 band compared with the G band and a considerable widening of the G-vibrational band. These changes in the Raman spectra once again strongly suggest a reduction in the size L_a of the coherent domain (“crystallites”) due to fast neutron flow while the reactor was in operation.

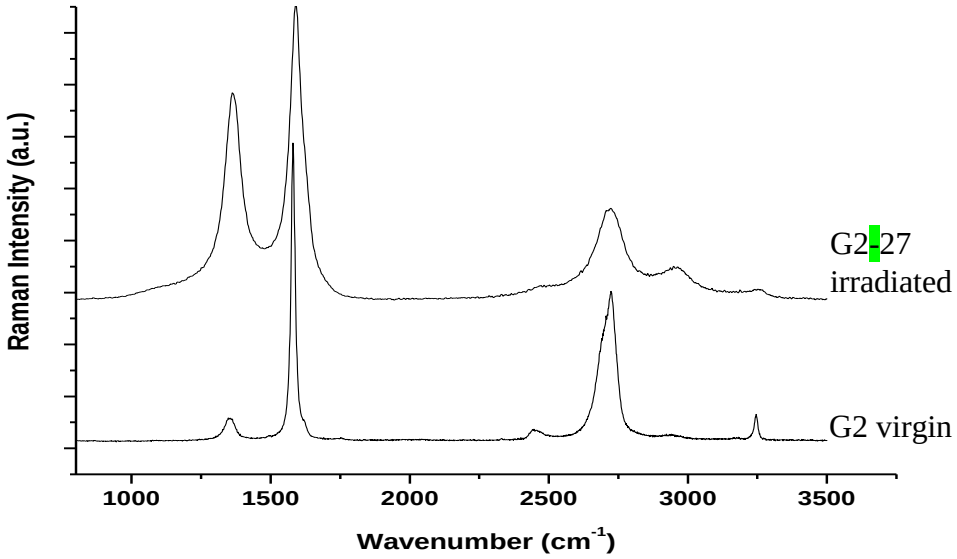

Figure 46 – Raman spectra of G2 virgin graphite and of G2 neutron-irradiated graphite (G2-27)

Quantitative analysis of the nuclear graphites through a decomposition of the Raman spectra (Figure 47), performed along the entire length of the radial sample core, shows that all the samples from the moderator have suffered almost the same structural damage ($\frac{I_{D_1}}{I_G}$ ~ 0.8; ~ 45 cm^{-1} for the G2 neutron-irradiated graphite and ($\frac{I_{D_1}}{I_G}$ ~ 0.09; $FWHM_G$ ~ 19 cm^{-1} for the G2 virgin graphite). This similarity in the degradation of the moderator is probably due to the similar irradiation temperatures (~ 300°C).

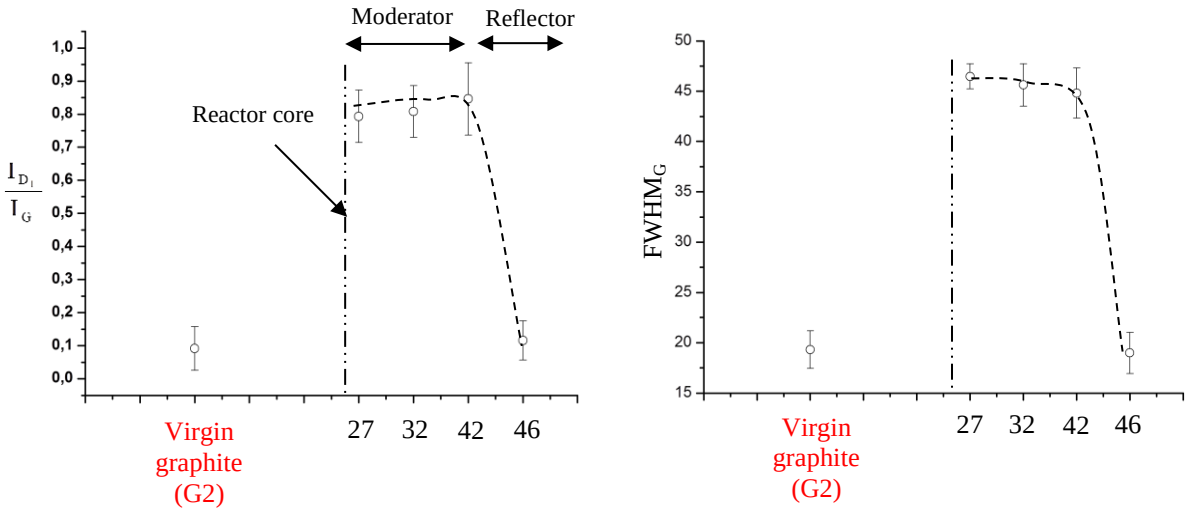

Figure 47 – Variations in the D1/G intensity ratio and in the full width at half maximum of the G band along the entire length of the radial core sample taken from the reactor.

It appears that the reflector suffered no significant structural damage, as demonstrated by the Raman parameters ($\frac{I_{D_1}}{I_G}$ ~ 0.11; $FWHM_G$ ~ 19 cm^{-1}) which are comparable to those obtained for the virgin graphite. Note that the values of L_a that can be calculated using the relation proposed by Tuinstra and Koenig (see page 13) are 49 nm for the virgin graphite, 5 nm for the irradiated graphites from the stack and 30 nm for the irradiated graphite from the reflector.

Characterisation using TEM

At the submicrometric scale, the irradiated graphites do not appear to differ very much from the virgin graphites. However, the lamellae are not as planar as in non-irradiated graphite (see Figure 26, p.29), and, at least in localised areas, lamellae may occur in fine folds as shown in the top image of Figure 48 below. Since the width of the folds (less than 10 nm in this case) is at least equal to the height L_c of the crystallites, this TEM image agrees with the decrease of L_c (widening of the 002 line) revealed using XRD. Photographs taken at greater magnification confirm these data. Thus, in these irradiated graphites, we observe 'fan-shaped'

textures that seem common and coherent domains that seem fragmented (Figure 46, bottom image).

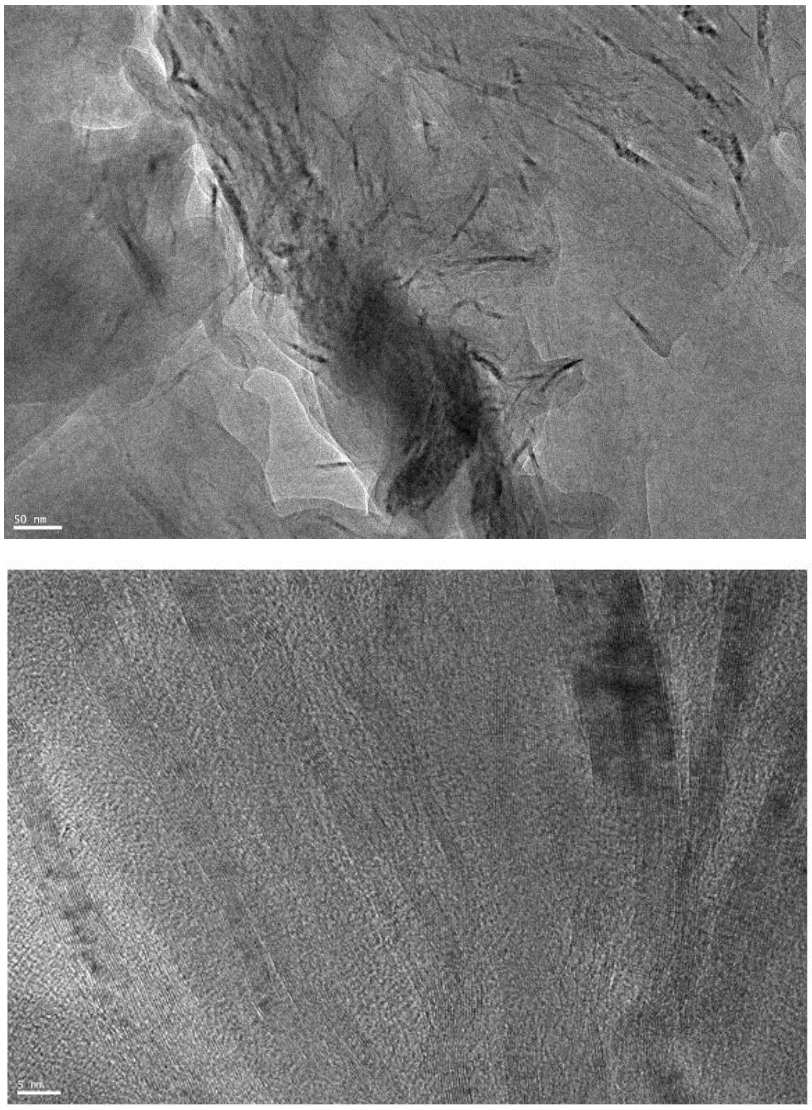

Figure 48 – TEM images of the G2 neutron-irradiated graphite (G2-27) (submicrometric scale) showing folded lamellae; a: bright field image; b: image of lattice fringes.

Still at the submicrometric scale, the analyses performed using transmission electron microscopy in 11(0) dark field mode reveal the crystalline structure to be extremely heterogeneous due to neutron irradiation. Figure 49 shows the example of Sample G2-27, characterised by the coexistence of coherent domains of different sizes. These range from around ten nanometres to around a hundred nanometres, i.e. from the typical size for virgin

graphite (image d) to around ten nanometres, typical of highly ‘destructured’ and, therefore, highly irradiated graphites (image a).

Such structural heterogeneity is also confirmed by the SAED diagrams given in the corner of each image below: we thus see a difference between a highly graphitised carbon for the large coherent domains (punctual hkl reflections, inset image d) and a turbostratic carbon for smaller domains (only slightly modulated hk bands can be seen in the location of hkl reflections in inset image a).

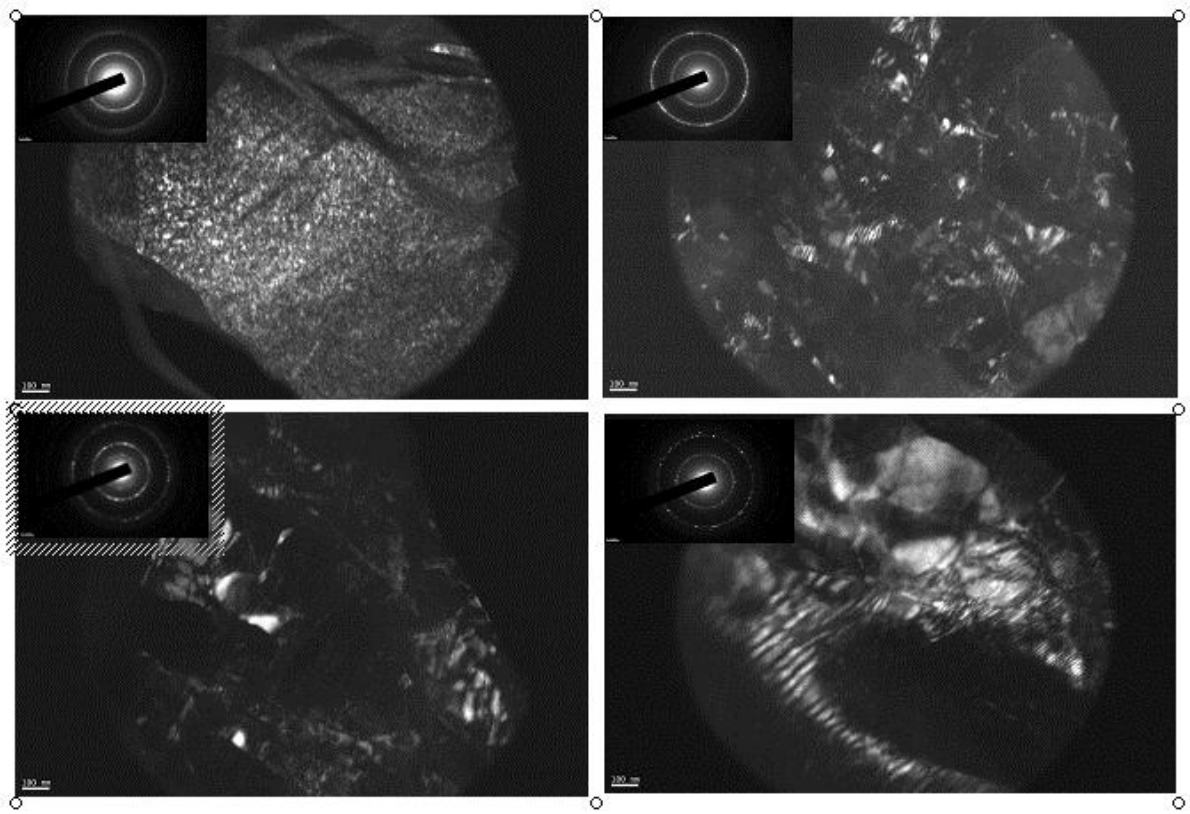

Figure 49 – Transmission Electron Microscopy images, 11(0) dark field mode, taken at various areas in Sample G2-27 of neutron-irradiated graphite, showing the heterogeneity, in terms of crystallite size, of this nuclear graphite. Inset image: SAED diagrams: a well-graphitised carbon (hkl reflexions), b and c: partially-graphitised carbons (modulated hk bands), d: completely turbostratic carbon (only hk bands).

In high resolution mode, we find two important information: (1) that the great heterogeneity of these carbons, detected using methods other than TEM, is conserved up to this

scale; (2) that the graphite's structural ordering is not always as clearly broken as might be expected on the basis of XRD or Raman integral analysis. It is thus relatively easy to find graphene planes that remain well stacked (Figure 50) in areas where large crystallites could be still seen in the 11(0) dark field images. We could nonetheless observe that, even at this well-organised stage, the layers are now slightly corrugated. The lateral extent of the coherent domains (perfectly stacked planar layers) is therefore not as large, which explains the increase in the D_1 band in the Raman spectra, and the broadening of the 002 lines, the maximum of which tending toward small angles as observed using XRD.

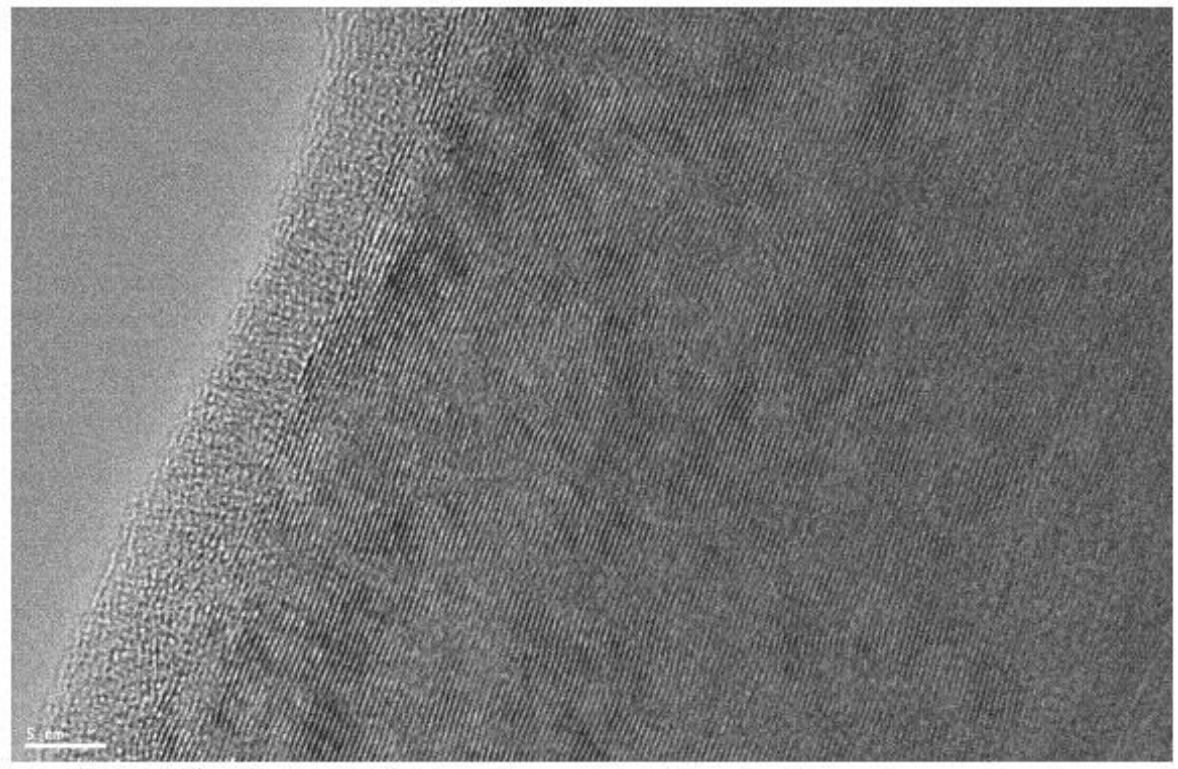

Figure 50 – High Resolution TEM image of neutron-irradiated nuclear graphite G2-27 showing low, but significant, degradation in the crystalline structure of the graphite.

However, in some places in the prepared sample, albeit apparently in the minority, extremely disordered carbons can be observed (HRTEM image, Figure 51 below).

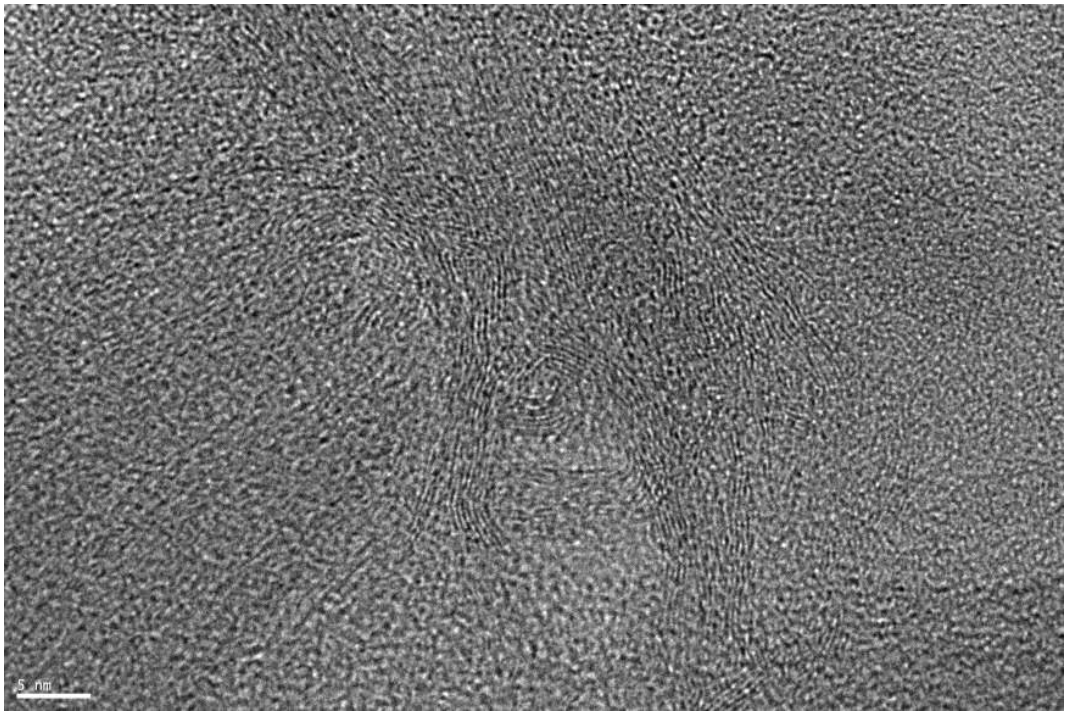

Figure 51 – High Resolution TEM image of neutron-irradiated nuclear graphite, sample G2-27, showing a strong degradation in the crystalline structure of the graphite: only badly-stacked, short layers that cause the occurrence of nanoporosity are now observed.

This image shows the most nanostructurally and structurally degraded areas. The lamellar nanostructure has practically disappeared, the layers are short (of nanometric size) and the stacks consist of only a few layers. All this causes the occurrence of nanoporosity. It is highly probable that these nanopores are potential sites for trapping contaminant elements such as ^{14}C and ^{36}Cl.

SLA2 nuclear graphite

The nuclear power plant site is located in St-Laurent Nouan, in Loir-et-Cher, on the edge of the left bank of the Loire River. It is approximately midway between Orléans (32 km to the northeast) and Blois (24 km to the southwest). The two gas-cooled (graphite-moderated) reactors (GCR) A1 and A2 at the Saint-Laurent plant are shown in the photograph below. They were commissioned in 1969 and 1971 and shut down in 1990 and 1992 respectively.

Within the framework of this contract, studies have been carried out on samples taken from the Saint-Laurent-des-Eaux reactor A2 (SLA2). This is a vertical reactor in which the coolant circulates from the top to the bottom of the core. In addition, the nearer the samples are to the top of the reactor, the more they are irradiated at low temperature (see Table 3 below).

PIT/SAMPLE	ALTITUDE	IRRADIATION TEMPERATURE
F10M16/ 43	1680 mm	400°C
F10M16/ 53	6500 mm	290°C
F10M16/ 60	9260 mm	240°C
F7M15/ 122	1080 mm	410°C
F7M15/ 129	4480 mm	340°C
F7M15/ 139	9260 mm	240°C

Table 3 - showing the position of the irradiated graphite core samples taken from the Saint Laurent reactor 2 (SLA2) and the corresponding irradiation temperatures.

X-ray diffraction

The behaviour of the irradiated graphite in SLA2 is very similar to that found for the irradiated graphites from the G2 reactor. The 002 line is displaced to small angles (i.e. an increase in inter-layer spacing) and there is significant broadening of the 002 reflection, indicating that the average height L_c of the coherent domains is smaller (see Figure 52 below). The results obtained show that the lower the irradiation temperature, the more degraded the graphite is. This agrees with the experiments that we carried out on ion-implanted graphites.

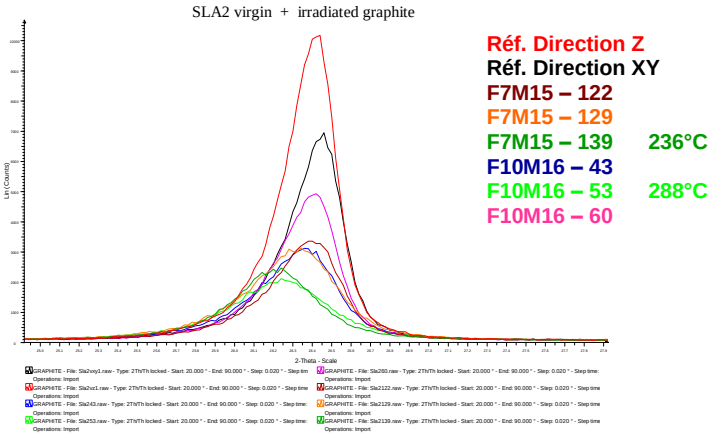

Pit F7M15

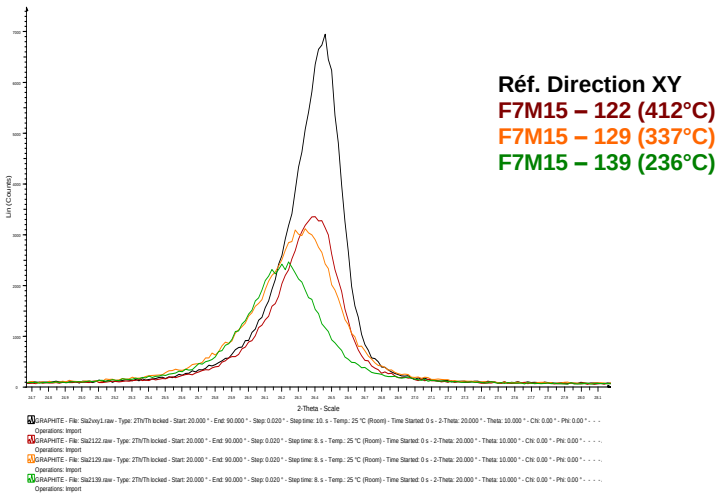

Figure 52 – 002 reflection profiles extracted from diffractograms performed on virgin and irradiated nuclear graphites from SLA2: top: all samples, bottom: samples from Pit F7M15.

Raman microspectrometry

The influence of the irradiation temperature is clearly demonstrated by the quantitative analyses of the Raman spectra (intensity ratios and full width at half maximum of the G band) as shown in Figure 53. The samples were taken from near the top of the reactor, and were thus subject to greater structural damage than samples taken toward the bottom, due to the direction in which the coolant gas circulated (from top to bottom).

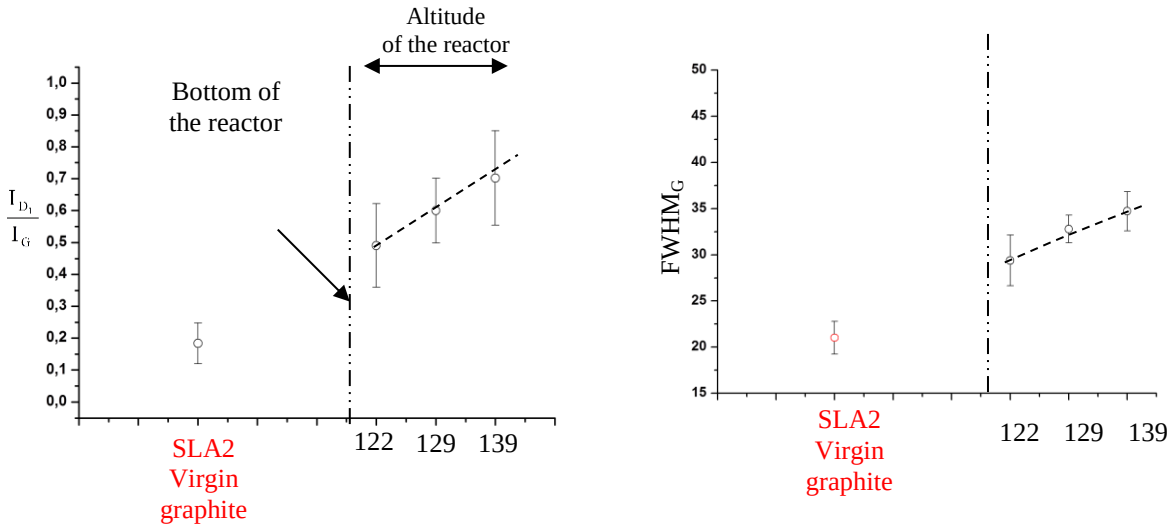

Figure 53 – Variations in the D1/G intensity ratio and in the full width at half maximum of the G band for the entire length of the vertical core sample taken from the reactor.

We previously demonstrated that the process of nuclear graphite restructuring by ion irradiation differs from its formation by pyrolysis. Once again, plotting the full width at half maximum of the G band versus the D_1/G intensity ratio either of the neutron- or of ion-irradiated graphites seems to show different behaviours (see Figure 54, next page). Ion irradiation does, certainly, cause a change in structure, although it is not exactly the same as the structural change caused by neutrons. Electron defects most likely add to structural defects during ion implantation of graphite.

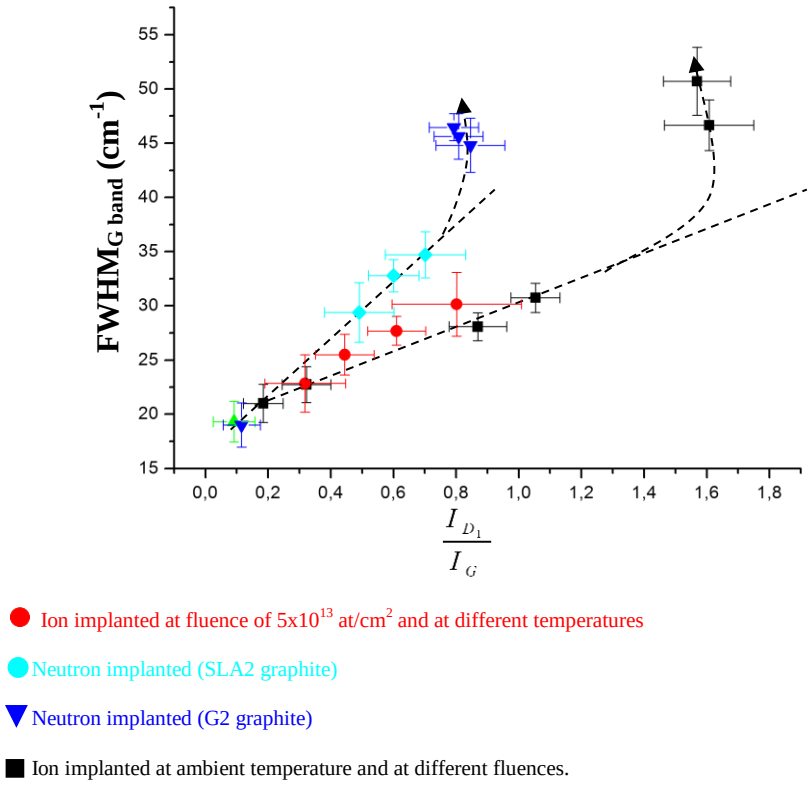

Figure 54 – Comparison of structural changes due to neutrons and to ions

Given the delay in obtaining the samples, characterisation using TEM of irradiated graphite from SLA2 is still in progress. However, our initial observations confirm those made for the irradiated graphite from G2. The carbons resulting from neutron irradiation remain very heterogeneous, but there is generally much less structural degradation than the amorphisation that can be observed during ion implantation of graphite at ambient temperature.

The respective effects of implantation with ^{37}Cl ions and neutron irradiation are illustrated in Figure 55 on the following page, which compares HRTEM images and semi-quantitative analysis of the images using the method proposed by J.N. Rouzaud and C. Clinard in 2002 [8].

The virgin graphite is characterised by large graphene layers (continuous across the area selected), which are perfectly stacked (the inter-layer spacing (0.338 nm) is very similar to the

theoretical value for graphite (0.3345 nm)). The structure of the graphite is more or less strongly disrupted depending on whether it was subject to ion implantation or neutron irradiation. Compared with the neutron-irradiated graphite, the graphite implanted with ^{37}Cl ions at ambient temperature and with fluence of ($5x10^{13}$ at/cm^2) seems to have undergone the greatest change: since the resulting layers are shorter (L = 0.8 nm rather than 1 nm) and more spaced (d = 0.42 nm rather than 0.37 nm). This carbon thus seems to be more nanoporous.

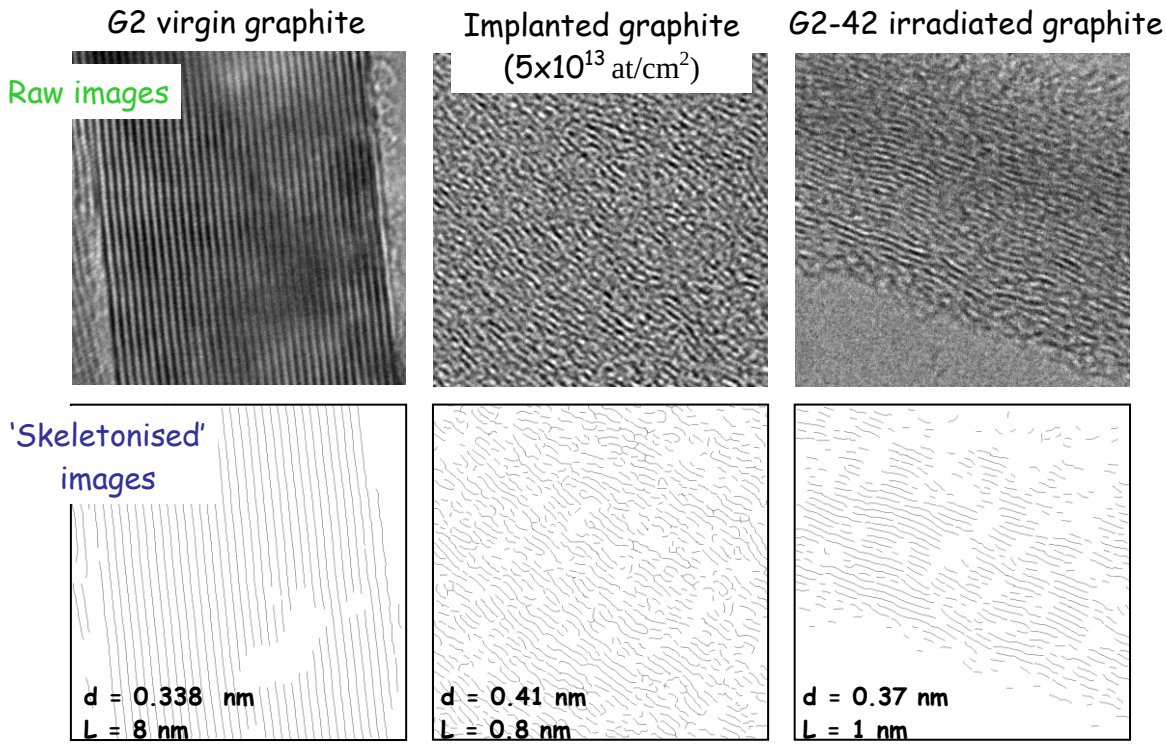

Figure 55 – 'Raw' HRTEM images (top) and skeletonised images (bottom) of the virgin graphite, graphite implanted with 37Cl ions at ambient temperature and with fluence of (5x1013 at/cm2) and of the neutron-irradiated graphite (size of images: 14 x 14 nm). Structural parameters based on image analysis; L: average length of layers in the area analysed, and d: average inter-layer spacing.

Conclusions regarding the study on the organisation of neutron-irradiated graphites from the SLA2 and G2 reactors

Having been irradiated when the nuclear reactors were in operation, the graphites have undergone structural changes. The results obtained by means of the three methods used to

characterise them (XRD, Raman and TEM) are convergent and demonstrate the development of disordering. The structural changes can be quantified using 'global' characterisation methods (XRD and Raman). Thus, the intensity of the Raman D_1 defect band increases, while the 002 reflection given by the diffractograms broadens and is displaced to small angles. This indicates, respectively, a decrease in width La and height Lc of coherent domains, and an increase in the average spacing between graphene layers. The ordering within these disrupted stacks is no longer bi-periodic, as shown by analysing the 10.0 and 10.1 reflections. TEM images, obtained using different modes (bright field, 11(0) dark field, high resolution and SAED) confirm these data and make it possible to visualise this increased disordering directly: we can directly observe, at least locally, the appearance of badly-stacked subnanometric layers. *This leads to the formation of nanopores which are most probably potential sites for trapping contaminants such as* ^{14}C *and* ^{37}Cl*.*

Nonetheless, the structure of these irradiated graphites is very heterogeneous and the majority of the areas observed seem to remain relatively undisturbed (using 11(0) dark field mode, large coherent domains can be seen to remain). Given such -somewhat surprising- heterogeneity at the µm-nm scales, it is not possible to obtain a reliable quantification of the TEM images, since the organisation can differ from one area to the next. While TEM affords the immense advantage of making it possible to directly visualise the most disordered areas, Raman and XRD are preferable when we wish to obtain data that are, at the least, semi-quantitative. However, it should be mentioned that the structural models of local defects and intercalation planes, based on a possibly inappropriate interpretation of XRD (computations based solely on the locations of 002 and 10.0 reflections of the carbonaceous stage, which is doubtless the most highly graphitised stage), appear to be somewhat simplistic in light of the High Resolution TEM images, which nonetheless make it possible to visualise the multiscale organisation of such complex irradiated graphite. Detecting the nanopores resulting from this structural disordering could, on the other hand, provide important new information, which can only be accessed using HRTEM.

Such a high degree of heterogeneity is caused partly by the very high heterogeneity of the carbon-carbon composite that we started with (a blend of quite highly-graphitised petroleum coke and probably less highly-graphitised pitch coke). In addition to this, there is most likely different behaviour between these carbon forms with regard to neutron irradiation: the most graphitised carbon may be more sensitive to the structural degradation.

The two neutron-irradiated graphites that we studied do not appear to have deteriorated to the same extent as certain ion-implanted graphites, which may, in certain cases (implantation with high fluence and at ambient temperature), be highly amorphised. If we compare the results obtained for the neutron-irradiated graphites from the G2 and SLA2 reactors with those obtained for the graphites implanted with ^{37}Cl ions at different temperatures, it is probably the relatively high temperatures to which these graphites were undergone inside the nuclear reactor that are responsible for their rather well-preserved structure and even their nanostructure. Although the tri-periodic ordering of the neutron-irradiated graphites is affected, as shown using both X-ray diffraction and Raman microspectrometry, their mechanical properties must have been relatively well preserved and the development of nanoporosity must have remained at much more limited level than would be the case in more extensive amorphisation. We can therefore make a distinction between layers that are merely wrinkled and between which contaminants can be trapped but where this can be reversed reasonably simply, and nanoporous carbons within which contaminant elements can be immobilised especially effectively.

7 General conclusion

This research study on virgin and irradiated nuclear graphite was carried out at the *Ecole Normale Supérieure*, Paris, within the framework of a contract with ANDRA and in collaboration with teams at the IPNL, CEA and EDF involved in the European ‘Carbowaste’ programme. The ENS Geology Laboratory (CNRS Joint Research Unit 8538) was tasked with characterising the multi-scale organisation of these nuclear graphites, before and after irradiation, using a combination of characterisation techniques, mainly Raman microspectrometry and Transmission Electron Microscopy (TEM), together with X-ray diffraction (XRD).

Our work concerns characterising the reference graphites (HOPG, natural graphite and various anthracene-based cokes, pitch- and petroleum-based cokes), graphites implanted with ^{37}Cl ions (in collaboration with the Institute of Nuclear Physics of Lyon, the IPNL) with a view to having non-radioactive analogues of irradiated graphite, together with virgin graphite and graphite that has been structurally changed by neutron irradiation inside the nuclear reactors in Saint-Laurent-des-Eaux (SLA2) and Marcoule (G2).

Compared with the state of knowledge when we started this study, we have made very significant progress in terms of developing original experimental approaches and new knowledge of these carbonaceous materials which, we hope, will have a significant impact on the disposal and/or the treatment of such materials, as well as making a contribution to resolving the problem of nuclear waste management.

With regard to progress in experimental methods and techniques, we have demonstrated that *Raman microspectrometry is a quantitative characterisation method -performed at the micrometer scale- which is particularly suited to characterising graphites and, above all, is particularly sensitive to detecting and quantifying structural defects generated by implantation or irradiation*. To do this, we developed an approach that enables us to propose a means of not introducing artefacts in the spectra due to the fact that graphites must first be polished in order to observe them using optical microscopy. We thus recommend using the full width at half maximum of the G band, which is more or less insensitive to surface condition. This approach has been presented at conferences in France (*Groupe Français d'Etude des Carbone*, Gréoux-les-Bains, 2009) and worldwide (Carbon 2010, Clemson University, USA).

We have also developed methods for cutting ultra-thin sections (<< 100 nm), in an SEM, using a Focused Ion Beam (FIB). *Thanks to these FIB sections, we were able to combine High Resolution TEM images with Raman microspectrometry images. This 'world first' is the subject of a paper published in 2010 in 'Carbon', the reference journal for carbonaceous materials*.

With our basic knowledge of carbonaceous materials and the approaches and methods specifically developed for this study, we have succeeded in making significant progress with regard to these materials and their management. First, we have confirmed that nuclear graphites are not, strictly-speaking, graphite, but carbon-carbon composites that are relatively highly graphitised (blend of petroleum coke grains and less highly graphitisable coal-tar pitch). Due to the method used to produce them, they are heterogeneous at both the micrometric and the nanometric scales, as our multi-scale approach demonstrates. This implies that they must not be confused with 'monocrystalline graphites', especially when they have been irradiated. We especially learned a great deal from the irradiation simulations that we carried out thanks to ^{37}Cl ion implantation at the INPL. These formally demonstrate the key role played by fluence, but also (and above all) by implantation temperature on the structure of implanted carbon. These results will be invaluable in developing our understanding of the damage caused by irradiation of nuclear graphites during reactor operating. Here too, *operating temperature is apparently a key factor*. This possibly explains why the two neutron-irradiated graphites that we examined (G2 and SLA2) do not seem to have deteriorated as much as some graphites implanted at high fluence and ambient temperature. *Our TEM images show the appearance, at least locally, of badly-stacked subnanometric graphene layers. The spatial disorientation of these small stacks leads to the formation of nanopores which are most probably potential sites for trapping contaminants such as ^{14}C and ^{37}Cl.* We can therefore make a distinction between areas where the layers are merely wrinkled (and between which contaminants can be trapped but where this can be reversed reasonably simply), and nanoporous carbons in the strict meaning of the term within which contaminant elements would be immobilised especially effectively. *This would seem to have important practical consequences with regard to the disposal and/or decontamination of nuclear waste*.

8 Outlook

The study carried out for the last two years under the Andra-ENS contract has greatly advanced our understanding of the structure of both virgin and irradiated graphites. Virgin graphites are highly graphitised carbon-carbon composites, but must not be confused with monocrystalline graphite, nor with the reference graphite, such as HOPG. The two irradiated graphite samples that we examined (G2 and SLA2) have undergone distinct structural change, as demonstrated using the three techniques implemented (Raman, TEM and XRD). In addition to the invaluable global analyses provided by XRD and Raman, the TEM shows the presence of more or less major disordering locally and, in particular, the occurrence of a highly disordered nanoporous carbon, quite different from the atomic models (based on somewhat 'simplistic' local defects, atoms and interstitial planes) previously deduced, possibly on the basis of a somewhat over-interpretation of X-ray diffractograms. *To follow on from this research, the next stage will obviously be to confirm the results obtained for G2 and SLA2 by examining other nuclear graphites irradiated under different conditions* (NPPs in Spain and the UK, etc.). *This could be performed via an amendment to this contract*.

9 References

[1] J.N. Rouzaud and A. Oberlin. Carbon, 27, 517-529, 1989.

[2] A. Oberlin, High-Resolution TEM Studies of Carbonization and Graphitization. In P.A. THROWER Ed 'Chemistry and Physics of Carbon', Volume 22, pp 1-143, 1991.

[3] J.N. Rouzaud, A. Oberlin and C. Beny-Bassez. Carbon films: Structure and microtexture (optical and electron microscopy, Raman spectroscopy). Thin Solid Films, 105, 75- 96, 1983.

[4] F. Tuinstra and J. Koenig, Journal of Chemical Physics 53, 1126, 1970.

[5] A. C. Ferrari and J. Robertson Phys. Rev. B 61, (2000) 14095–14107

[6] Warren BE. X-ray diffraction methods. J Appl Phys 1941; 12:375–83

[7] Salver-Disma F, Tarascon JM, Clinard C, Rouzaud JN.Carbon 1999; 37:1941

[8] J.N. Rouzaud and C. Clinard (2002). Fuel Processing Technology, 77-78 (2002), 229-235.

10 Papers published as a result of this study

C.E. VAUDEY, N.TOULHOAT, N.MONCOFFRE, N.BÉRERD, L.RAIMBAULT, P.SAINSOT, J.N.ROUZAUD, A.PERRAT-MABILON (2009). Thermal behaviour of chlorine in nuclear graphite at a microscopic scale, *Journal of Nuclear Materials* 395 (1-3), 62-68.

M.R. AMMAR, J.N. ROUZAUD, C.E.VAUDEY, N. TOULHOAT, AND N. MONCOFFRE (2010). Multiscale characterization of implanted graphite by coupling Raman microspectrometry and Transmission Electron Microscopy using the FIB thin sections, *Carbon* 48(4), 1244-1251.

M.R. AMMAR and J.N. ROUZAUD (2011). How can Raman microspectrometry be used to obtain quantitative structural characterization on polished graphitised carbons?. Paper in press for Journal of Raman Microscopy.

M.R. AMMAR, J.N. ROUZAUD, C.E. VAUDEY, N. TOULHOAT, N. MONCOFFRE. Characterization of graphite implanted with chlorine ions using combined Raman microspectrometry and Transmission Electron Microscopy. Paper currently being drafted for Carbon.

M.R. AMMAR, J.N. ROUZAUD, L. GOSMAIN. Characterization of virgin and irradiated nuclear graphite. Paper currently being drafted for Carbon or the Journal of Nuclear Materials.

11 Communications made under the contract

In addition to the communications made at meetings of the European Carbowaste programme (Berlin 20-22 January 2009, Paris, 30 March 2009, Madrid, 9-10 June 2009, Vandellos 27-28 April 2010 (guest presentation), and at 'Graphite' GT (Technical Group) meetings (Moret-sur-Loing, 29 March 2007; Saclay, 2008, Bures, 12-13 October 2009 ; Saclay 11 March 2010; Marcoule, 20-21 September 2010) and to the *Groupe Français d'Etude des Carbones* (GFEC, Gréoux-les-Bains, 29 March – 1 April 2010), this research has been presented at the last two 'Carbon' international conferences and at the 'International Nuclear Graphite Specialists Meeting (INGSM)' in 2008 and 2009:

J.N. ROUZAUD, C.E. VAUDEY, N. TOULHOAT, N. MONCOFFRE (2008). Characterization of nuclear graphites by Raman microspectrometry and TEM; preliminary results. 9th International Nuclear Graphite Specialists Meeting, Egmond aan Zee, 17 September 2008.

M.R. AMMAR, C.E. VAUDEY, J.N. ROUZAUD, N. TOULHOAT, N. MONCOFFRE (2009). Characterization of virgin and implanted nuclear graphites. The Annual World Conference on Carbon, Biarritz, 14-19 June 2009.

M.R. AMMAR, J.N. ROUZAUD, C.E. VAUDEY, N. TOULHOAT, N. MONCOFFRE (2009). Structural study of implanted nuclear graphite used to simulate irradiation effects. 10th International Nuclear Graphite Specialists Meeting, West Yellowstone, USA, 28-30 September 2009.

M.R. AMMAR, J.N. ROUZAUD, C.E. VAUDEY, N. TOULHOAT, N. MONCOFFRE (2010). Structural study of ion beam irradiation of nuclear graphite. The Annual World Conference on Carbon, Clemson (NC, USA), 11-16 July 2010.